Interactome analyses reveal profound proteasome structural and functional rearrangements throughout mammalian spermatogenesis

Dušan Živković[1], Angelique Sanchez Dafun[1], Thomas Menneteau[1], Adrien Schahl[1], Sandrine Lise[1], Christine Kervarrec[2,3], Ana Toste-Rêgo[4,5], Paula C. A. da Fonseca[4,5], Matthieu Chavent[1], Charles Pineau[2,3], Odile Burlet-Schiltz[1], Julien Marcoux[1]* and Marie-Pierre Bousquet[1]*

[1]Institut de Pharmacologie et de Biologie Structurale, Université de Toulouse, CNRS, UPS, 3100 Toulouse, France.
[2]Univ Rennes, Inserm, EHESP, Irset (Institut de recherche en santé, environnement et travail) - UMR_S 1085, 35042 Rennes cedex, France.
[3]Protim, Univ Rennes, 35042 Rennes cedex, France.
[4]MRC Laboratory of Molecular Biology, Francis Crick Avenue, Cambridge CB2 0QH, UK.
[5]Institute of Molecular, Cell and Systems Biology, University of Glasgow, UK.
*To whom correspondence should be addressed. Email: julien.marcoux@ipbs.fr; marie-pierre.bousquet@ipbs.fr

Abstract

During spermatogenesis, spermatogonia undergo a series of mitotic and meiotic divisions on their path to spermatozoa. To achieve this, a succession of complex processes requiring high proteolytic activity are in part orchestrated by the proteasome. The spermatoproteasome (s20S) is a proteasome subtype specific to the developing gametes, in which the gamete-specific α4s subunit replaces the α4 isoform found in the constitutive proteasome (c20S). Although the s20S is conserved across species and was shown to be crucial for germ cell development, its mechanism, function and structure remain incompletely characterized. Here, we used advanced mass spectrometry (MS) methods to map the composition of proteasome complexes and their interactomes throughout spermatogenesis. We observed that the s20S becomes highly activated as germ cells enter meiosis, mainly through association with proteasome activators PA200 and 19S. Additionally, the proteasome population shifts from predominantly c20S (98%) to predominantly s20S (>82-92%) during differentiation, presumably due to the shift from α4 to α4s expression. We confirmed that s20S, but not c20S, interacts with components of the synaptonemal complex, the multi-protein assembly that connects homologous chromosomes during meiosis. *In vitro*, s20S preferentially bind to 19S, and displayed higher trypsin- and chymotrypsin-like activities, both with and without PA200 activation. Moreover, using MS methods to monitor protein dynamics, we identified significant differences in domain flexibility between α4 and α4s. We propose that these differences induced by α4s incorporation result in significant changes in the way the s20S interacts with its partners, and dictate its role in germ cell differentiation.

Introduction

Spermatogenesis is a process of cell differentiation, whereby a part of the population of stem cells called spermatogonia (SPG) enter the differentiation pathway and develop into spermatids, which then enter the spermiation process to become fully developed spermatozoa. Spermiogenesis is the differentiation of haploid round spermatids into elongated spermatids. During this maturation, a number of cell remodeling events are completed, including several critical cell-specific remodeling processes such as DNA condensation, mitochondrial reorganization, production of the flagellum and cytoplasm removal (Calvel *et al.*, 2010). SPG first divide mitotically and develop into spermatocytes (SPC), which enter meiosis. Meiosis requires duplication of the genetic material, its condensation, recombination between the maternal and paternal homologue chromosomes and re-distribution of the recombined chromosomes into separate cells. This is immediately followed by another division resulting in daughter cells called spermatids (SPT) with only one recombined copy of each chromosome. This entire process is facilitated by the Sertoli cells (SER) that serve to support developing gametes (Holstein, Schulze and Davidoff, 2003). Recombination is a particularly lengthy process requiring the formation of special bridges across paired chromosomes, called synaptonemal complexes (SCs), which enable the exchange of parts of chromosomes (Hunter, 2015). Overall, spermatogenesis and spermiogenesis are both proteolysis-intensive processes with high protein turnover that require intense engagement of the primary proteolytic machinery of the cell, the proteasome (Hou and Yang, 2013).

The proteasome is a macromolecular proteolytic machinery in charge of controlled degradation of proteins (Collins and Goldberg, 2017). The proteasome core, also known as the 20S proteasome, is a symmetric, barrel-like structure that consists of a catalytic chamber formed by β subunits, which is sealed on both ends by a ring of α subunits (Bousquet-Dubouch et al., 2011; Collins and Goldberg, 2017; Sahu and Glickman, 2021). The 20S associates with various proteins and protein complexes, the most notable being the proteasome activator complexes 19S regulatory particle (to form the 26S proteasome), PA28αβ, PA28γ and PA200. These regulators modify the 20S activity and substrate specificity in order to regulate various processes such as cell division, differentiation, heat shock response, DNA repair, immune response, apoptosis, and many others (Aristizábal *et al.*, 2019; Kloetzel, 2004, Min and Lindon, 2012; Qian *et al.*, 2013; Sohn *et al.*, 2006; Widjaja *et al.*; 2017; Zhang *et al.*, 2019). Moreover, the proteasome complexity is further increased by the presence of several proteasome subtypes where one or several subunits of the constitutive complex are replaced by alternative isoforms. Thus far, in addition to the constitutive 20S proteasome (c20S), immuno- (i20S), thymo- (t20S), and spermato-proteasomes (s20S) have been identified and described in the literature (Kniepert and Groettrup, 2014).

The s20S is a proteasome subtype in which the standard α4 subunit (PSMA7 gene) is replaced by α4s (PSMA8 gene) that is expressed exclusively in gamete cells (Kim et al., 2014). Previous studies in PSMA8$^{-/-}$ KO mouse models have established that the α4s subunit is essential for spermatogenesis (Gomez-H *et al.*, 2019; Zhang *et al.*, 2019). Functionally, mammalian s20S has been shown to degrade acetylated histones via association with PA200 and play a role in DNA damage repair in spermatocytes and the maturation of spermatids (Qian *et al.*, 2013; Zhang *et al.*, 2019, 2021). Double strand break (DSB) repair was shown to be dependent on s20S-mediated degradation of non-histone substrates (Ahuja *et al.*, 2017; Zhang *et al.*, 2021). Cell cycle-mediating proteins were also reported as substrates of s20S (Bassermann, Eichner and Pagano, 2014; Gao *et al.*, 2019). However, despite these reports, s20S remains understudied and there is currently a lack on basic information on the exact nature and relative stoichiometry of the regulators binding to the s20S during spermatogenesis. In this context, revealing the dynamics of the 20S proteasome composition and partners throughout spermatogenesis could help explain how the s20S functions are conveyed, and further elucidate the underlying molecular mechanisms.

Here we use advanced mass spectrometry (MS)-based approaches to map interactomes of mammalian s20S during male germ differentiation and compare them with those of c20S. Our analyses in whole testes and in isolated male germ cells revealed specific s20S partners and profound changes in the dominant 20S proteasome subtypes present throughout differentiation. Incorporation of α4s into s20S was strikingly correlated with an increased association with 19S, PA200 and PI31 regulators, and with an overall proteasome activation, especially regarding its trypsin- and chymotrypsin-like activities. Moreover, using hydrogen-deuterium exchange (HDX)-MS and molecular dynamics simulations we identified conformational differences between α4 and α4s, providing a molecular rationale for the observed differences between c20S and s20S.

Results

Top-down MS reveals the proportion of s20S in mammalian testes

To examine differential expression patterns of s20S and c20S, as well as other proteasome-associated factors, we analyzed tissue-specific human proteome maps (Kim *et al.*, 2014) and observed that the expression pattern of the PA200 and 19S regulators closely follows that of α4s (**Supplementary Fig. S1A**). We noted that both male and female gonads express s20S (**Supplementary Fig. S1A**), but given that the only reported role for s20S is in male germ cells we decided to focus our analysis on whole testes and purified male germ cells. This does not exclude that the s20S may play a still unknown role in females.

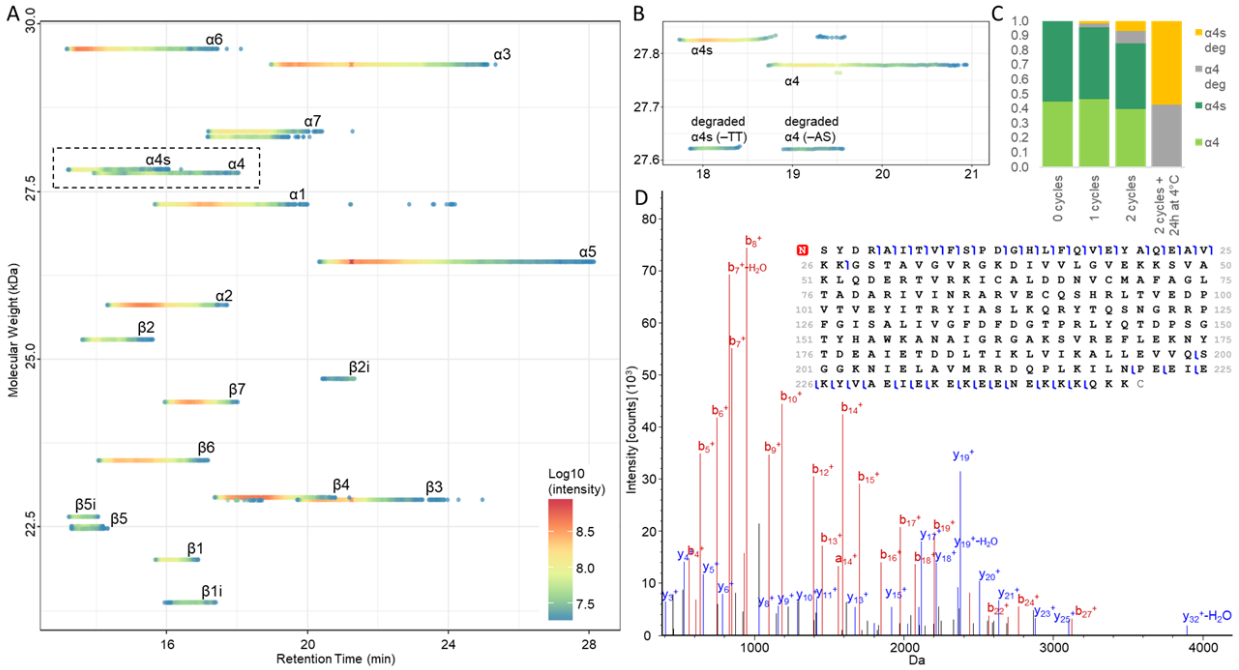

Figure 1. **(A)** 3D proteoform footprint of the LC-MS trace of 20S subunits immunopurified from bovine testis, generated with VisioProt-MS (Locard-Paulet *et al.*, 2019). The names of the c20S subunits are indicated next to the corresponding signal. **(B)** Close-up view of the 3D proteoform footprint of 20S subunits immunopurified from bovine testes after repeated freeze-thaw cycles, resulting in truncated proteoforms of α4 and α4s. **(C)** The truncated α4 and α4s to the full-length proteins ratio increase with repeated freeze-thaw cycles. **(D)** Top-down LC-MS/MS of α4 identifies the degradation as the loss of the last two amino-acids.

To map the relative abundance of s20S, we used freshly frozen bovine testis lysate where the s20S is highly expressed. We immunopurified (IP-ed) 20S proteasome using the MCP21 antibody that recognizes the α2 proteasome subunit (present in all 20S proteasome subtypes), as described previously (Fabre *et al.*, 2015). The 20S proteasome was then further separated from its regulators by an additional Size Exclusion Chromatography (SEC) step (Sbardella *et al.*, 2018). After IP and SEC, the purified 20S proteasomes were analyzed on a LC-MS system, using a previously optimized method (Lesne *et al.*, 2019). We were able to identify not only the proteasome subunits that are conserved among the different 20S subtypes, but also the specific catalytic subunits of the c20S (β1, β2, β5) and the i20S (β1i, β2i, β5i), as well as the testes-specific α4s subunit of the s20S (**Fig. 1A**; **Supplementary Table 1**). Taking the β5 subunit abundance as reference, the results show that most of the 20S proteasomes in testis contain exclusively the three constitutive catalytic subunits (64% ± 1 %), while some complexes with different combinations of constitutive and immune subunits are also present (Guillaume *et al.*, 2010; Fabre *et al.*, 2014) (**Supplementary Table 1)**. Additionally, we could quantify the proportion of s20S using the MS signals of α4 *vs.* α4s subunits, by assuming that they

have similar ionization yields based on their high sequence identities (**Supplementary Fig. S1B**). In this way we established that the s20S constitutes 48 ± 1 % of the total testis immunopurified proteasomes, which will thereafter be called “testes 20S pool”.

Table 1. Theoretical and observed MWs of the bovine proteasome subunits, along with their corresponding PTMs *nomenclature as in (Baumeister *et al.*, 1998).

Name*	Theoretical MW (mature isoform)	Theoretical MW (with PTMs)	Observed mass	Modification	Δm
α1	27399.5	27310.5	27308.7	-Met+Ac	-1.8
α2	25767.4	25809.4	25807.8	+Ac	-1.6
α3	29483.8	29394.8	29393.2	-Met+Ac	-1.6
α4	27868.9	27779.9 27621.7	27777.5 27620.7	-Met+Ac -Met+Ac-AS	-2.4 -1.0
α4s	27915.0	27826.0 27623.6	27825.1 27622.5	-Met+Ac -Met+Ac-TT	-0.9 -1.1
α5	26411.0	26453.0	26451.9	+Ac	-1.1
α6	29585.6	29627.6	29626.0	+Ac	-1.6
α7	28274.0	28396.0 28316.0	28394.2 28314.9	+Phos+Ac +Ac	-1.8 -1.1
β1	22010.1	22010.1	22009.0	-	-1.1
β1i	21373.2	21373.2	21371.7	-	-1.5
β2	25292.0	-	25291.3	-	-0.7
β2i	24709.3	24709.3	24707.9	-	-1.4
β3	22861.7	22903.7	22902.5	+Ac	-1.2
β4	22896.3	22938.3	22937.1	+Ac	-1.2
β5	22474.3	22474.3	22472.6	-	-1.7
β5i	22632.7	22 648.7	22649.0	+Ox	+0.3
β6	23490.9	-	23489.6	-	-1.3
β7	24361.8	24361.8	24360.4	-	-1.4

In addition to quantifying different proteasome species, we were able to observe various PTMs (summarized in **Table 1**), that were in accordance with published data (Thompson, Schaeffer-Reiss and Ueffing, 2008; Lesne *et al.*, 2019; Vimer *et al.*, 2020). Interestingly, we noticed that α4s harbors the same PTMs as the α4 proteoform, *i.e.* loss of the initial methionine and N-terminal acetylation. Additionally, we observed that repeated freeze-thaw cycles led to formation of truncated versions of α4 and α4s subunits

that lack the last two amino acid residues (**Fig. 1B-C**), which were later confirmed by LC-MS/MS Top-Down (TD) sequencing (**Fig. 1D**). A similar loss in mass, corresponding to a truncated version of α4, was recently described in rat and rabbit (Vimer *et al.*, 2020). Given that our results indicate that these lighter α4/α4s isoforms are produced upon storage, most likely via proteolytic cleavage of their solvent accessible C-termini, we consider them unlikely to be biologically relevant. We also noted +73 Da and -13 Da mass differences observed for β6 and β2, respectively (**Supplementary Fig.S2**). TD sequencing confirmed that in our sample these subunits differ from the official (curated) Swiss-Prot entries by 1 amino-acid (G233E for β6 and N252T for β2) but are in agreement with predicted TrEMBL entries. These mutations are barely visible using bottom-up proteomics where proteins are commonly identified with only a few peptides, illustrating the benefits of TD-MS for proper proteoform characterization and database curation. Taken together, our TD-MS analysis of the immunopurified proteasome pool from bovine testes revealed that s20S represents a major fraction of the total proteasome, suggesting a key functional role.

Specific set of interactors of the s20S in bovine testes

To further characterize the s20S in gamete cells, we mapped its interactome using an IP strategy. We performed two IPs from bovine testes lysates using either an anti-α4s-specific antibody (generated according to Uechi, Hamazaki and Murata, 2014, and validated as shown in **Supplementary Fig. S3**), which targets only the s20S, or an anti-α2 antibody, which recognizes all proteasome types, and compared the relative abundances of co-immunopurified proteins. In a first set of experiments, lists of proteasome interacting proteins (PIPs) specific to α2 and α4s were obtained by comparing the anti-α2 or anti-α4s IPs against a control IP (antibody directed against rat CD8- OX8, as used previously (Bousquet-Dubouch *et al.*, 2009)). 3867 proteins were validated and quantified in the anti-α2 and anti-α4s IPs, with a total of 1177 proteins exhibiting over a 2-fold change (FC) enrichment (significance threshold at $p<0.05$) compared to the control (**Supplementary Fig. S4, S5**). To highlight putative specific or enriched components in c20S and s20S interactomes, we compared the relative abundances of each of these proteins in the anti-α2 IP (total 20S) *vs.* anti-α4s IP (s20S). To do so, protein abundances were normalized based on the 20S content in each IP (estimated as the average of the abundances of the non-catalytic 20S subunits), then the fold changes (anti-α4s IP / anti-α2 IP) and their significance (*p*-value) were calculated and represented as a Volcano plot (**Fig. 2A**). Here an unequal distribution of enriched proteins is observed, skewed towards the anti-α4s IP. One possible explanation for this observation is that the anti-α4s antibody might fetch 20S interactors that appear below the detection threshold when analyzing the whole 20S interactome (*i.e.,* with the anti-α2 antibody only). However, we also acknowledge that the anti-α4s polyclonal antibodies used may display more non-specific bindings, compared to monoclonal antibodies used

in the anti-α2 IP. We therefore looked specifically at proteins that might be of interest, namely proteasome- and ubiquitin-related proteins.

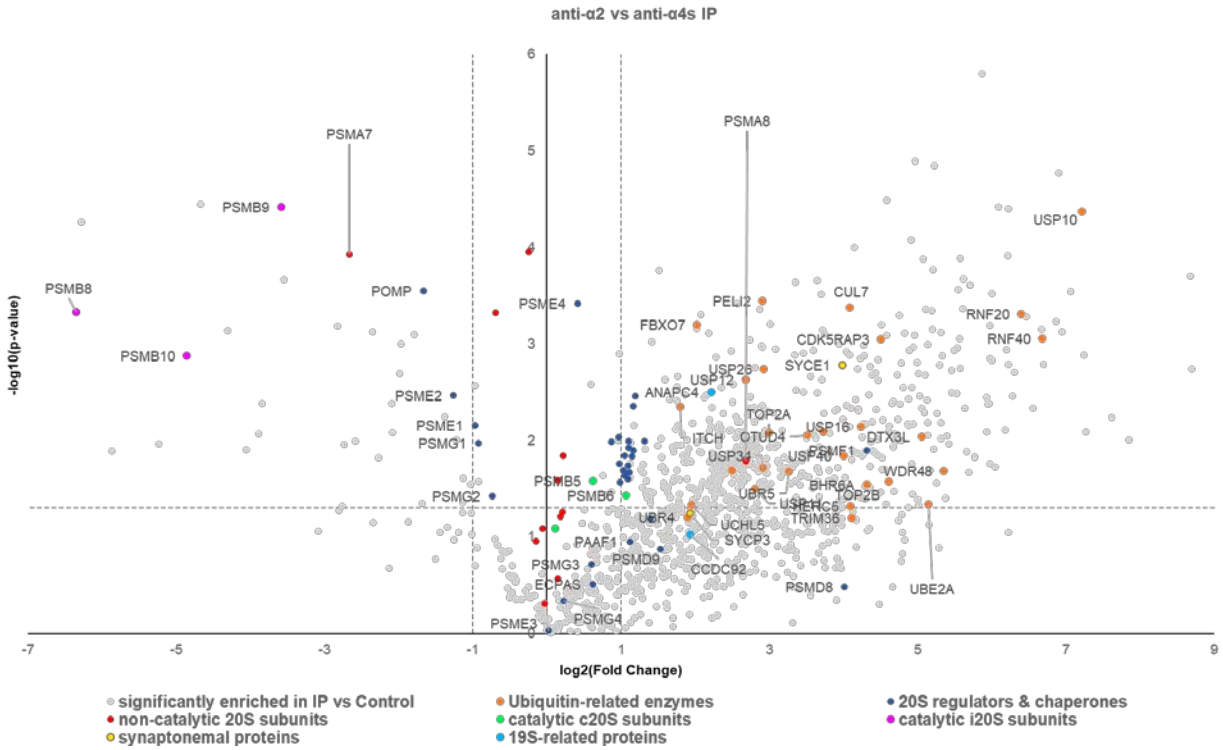

Figure 2. Analysis of proteasome composition and interacting proteins in bovine testes. **(A)** Distribution of enriched proteins between two IPs against anti-α2 (left hand side) and anti-α4s (right hand side). Only proteins that were enriched (FC>2, *p-value* <0.05) in the anti-α2 or anti-α4s IPs compared to the control IPs are displayed here. For clarity, gene names are used as protein identifiers. **(B)** Estimated percentages of α4 and α4s in the different IPs. The protein intensities were normalized based on the 20S content and the relative abundances of α4 and α4s estimated for the different IPs (anti-α4s, anti-α2, and anti-PA200). **(C)** FCs of 20S-associated regulators in the s20S (α4s-containing proteasome) relative to α4-containing proteasomes. The relative quantities of α4 and α4s in the anti-α4s and anti-α2 IPs enables to estimate the fraction of 20S-associated regulator in the α4s- and α4-containing proteasomes. Finally, FCs in α4s- *vs.* α4-containing proteasomes were calculated, as detailed in the experimental section. Graphics represent mean and standard deviations. All values are the means of three independent experiments. Stars indicate significance. * : p<0.05; **: p<0.01; ***: p<0.001.

The distribution displayed on **Fig. 2A** highlights the specific composition features of c20S and s20S complexes. Only proteins that were enriched (FC>2, *p-value* <0.05) in anti-α2 or in anti-α4s IPs compared to the control IPs are displayed in this comparison. We observed that the non-catalytic 20S subunits (except α4 and α4s - PSMA7 and PSMA8 genes, respectively) are found tightly centered around the y-axis (mean FC = 1.0 +/- 0.2), showing that the normalization of the dataset is well done and that there are no

major variations in their relative abundance. As expected, the bait of the anti-α4s IP is found on the right (α4s protein - PSMA8, FC = 6.4, *p-value* = 0.016) whereas the subunit replacing it in the c20S is found on the left (α4 protein - PSMA7 gene, FC = 0.16, *p-value* = 12.E-4). We then used the relative abundances of the α4 (PSMA7) and α4s proteins (PSMA8) in the anti-α2 IP to estimate the part of s20S in the total pool of 20S proteasome in bovine testis (42 ± 7%; **Fig. 2B**), which is in good agreement with the results obtained by the TD approach. On the other hand, the anti-α4s IP contains 95 ± 9% of s20S (**Fig. 2B**), confirming the exclusive nature of the α4s subunit incorporation into the s20S (Zhang *et al.*, 2019) (Gomez-H *et al.*, 2019). Taken together, our data provide evidence that the α4s and α4 subunits do not co-exist within a hybrid 20S proteasome. This subunit exclusivity is in agreement with what has been previously observed for some i20S catalytic subunits (Griffin *et al.*, 1998) (Kingsbury, Griffin and Colbert, 2000), and could result from exclusive expression of either the α4 or the α4s.

We observed that the three i20S-specific catalytic subunits (PSMB8-10 proteins, **Fig. 2A**) were more abundant in the anti-α2 IP and were practically absent from the anti-α4s IP, implying that no immuno-subunits constitute the s20S (FC of immuno subunits in anti-α4s IP = 0.006, *p-value* = 7.E-5, **Fig. 2C**), as previously observed using an orthogonal immunodetection approach (Gomez-H *et al.*, 2019). This interesting result is also in agreement with the 6.1 fold decrease, in the anti-α4s IP, of PA28αβ (*p-value* = 0.01), known to interact preferentially with the i20S (Fabre *et al.*, 2015). Moreover, while the four 20S Proteasome Assembly Chaperones (PAC) are equally distributed in the α4- and α4s-containing 20S (**Fig.3A, Supplementary Table 2**), the POMP maturation protein is 5.3 fold increased in the α4-containing 20S (*p-value* = 0.02, **Fig.3C, Supplementary Table 2**). POMP is known to preferentially promote the assembly of i20S catalytic subunits over c20S ones (Griffin *et al.*, 1998; Heink *et al.*, 2005; Johnston-Carey, Pomatto and Davies, 2016), which agrees with our observation that immuno-catalytic subunits are low abundant in the anti-α4s IP.

Our analysis of main 20S interactors revealed that all subunits of the 19S particle could be quantified and their very tight distribution in the Volcano plot (*i.e.* very close FCs and *p-values*, **Fig. 2A**) emphasizes the quality of this dataset. Interestingly, we could measure an average increase of 2.13 ± 0.15 of 19S subunits in the anti-α4s IP compared to the anti-α2 IP. Since the anti-α4s antibody purifies almost exclusively α4s-containing 20S (95 ± 9%) and the anti-α2 IP contains a mix of proteasomes (42% of α4s-containing 20S), we can estimate that in whole testes, the abundance of the 19S bound to the s20S is approximately 15 times higher than the one associated with the c20S (*p-value* = 0.02) (**Fig. 2C** and **Supplementary Table 2**). Interestingly, other known 19S interactors were also found to be increased in the anti-α4s IP compared to the anti-α2 IP. This is the case for the two main 19S-associated deubiquitinases USP14 and UCHL5 (FC = 3.2 and 3.9, *p*-values = 0.02 and 0.05, respectively), ADRM1 protein, a known 19S receptor of

polyubiquitin chains (FC = 1.8, *p*-value = 0.01), as well as RPS27, the main cellular precursor of ubiquitin (FC = 1.9, *p*-value = 0.03). The K48 polyubiquitin chains identified by the LIFAGK(GG)QLEDGR peptide (Døskeland, 2006) were increased by a factor of 3.0 (*p*-value = 0.001) in the anti-α4s IP compared to the anti-α2 IP. Altogether this dataset suggests a higher loading of polyubiquitinated substrates onto s20S compared to total proteasome complexes. Accordingly, among the 40 ubiquitin-related enzymes (conjugating enzymes, ligases and deubiquitinylases) that are found significantly regulated between the two IPs, all were increased in the s20S interactome except TRIM21, an E3 ligase that is mainly involved in immune response (**Supplementary Table 3**).

Another PIP found to be highly regulated in this dataset is PI31, a 20S interactor of controversial function (Li *et al.*, 2014). PI31 displayed a 20-fold enrichment in the anti-α4s IP compared to the anti-α2 IP (**Fig. 2A**, *p-value* = 0.01) and seems to be a preferred partner of the s20S (**Fig. 2C and Supplementary Table 2**). Strikingly, a known heterodimerization partner of PI31, Fbxo7 (Kirk *et al.*, 2008), is also significantly more abundant in the s20S IP (FC 72; *p-value* = 0.007). Recent KO studies of Fbxo7 and Nutcracker, its heterolog in drosophila, indicate important roles of both proteins during spermatogenesis (Rathje *et al.*, 2019; Bader *et al.*, 2011). Due to the established role of PA200 in spermatogenesis (Qian *et al.*, 2013), a complementary IP directed against PA200 also show that PI31 and Fbxo7 proteins are also highly enriched in the anti-α4s IP compared to the PA200 IP (FCs = 12.2 and 4.1, *p-values* = 1E-04 and 0.05, respectively, **Supplementary Fig. S6, S7**), suggesting that these proteins are directly linked to the s20S and not bound to it through an interaction with PA200.

We found that the synaptonemal proteins SYCP3 and SYCE1 are specifically enriched in the anti- α2 and anti-α4s IPs, compared to their respective control IP (**Supplementary Fig. S4 & S5**), and significantly more abundant in the s20S interactome compared to the other α4-containing 20S isoforms (FCs = 294 and 3.8, respectively; *p-values* = 8E-03 and 0.05, respectively (**Fig. 2A, 2C and Supplementary Table 2**). Previous imaging studies have suggested that these proteins interact directly with the s20S (Gomez-H *et al.*, 2019), and our dataset further supports such specific interactions of the s20S with the SC.

Despite their proposed role in spermatogenesis (Huang *et al.*, 2016), the nuclear PA28γ and PA200 regulators of the 20S core were either not (FC = 0.8; *p-value* = 0.4) or only slightly, but still significantly (FC = 2.0; *p-value* = 0.03), enriched in the s20S compared to the α4-containing 20S subtype (**Fig. 2C and Supplementary Table 2**). Moreover, when comparing the relative abundances of α4 and α4s co-purified in the anti-α2 and in the anti-PA200 IPs, we observed similar values (**Fig. 2B**). Altogether, these results suggest that PA200 may not interact preferentially with the s20S, contrary to what

was previously speculated (Kniepert and Groettrup, 2014). However, if the α4 and α4s isoforms are expressed in different cell types, as previously reported (Zhang *et al.*, 2019), they would not have to compete for PA200 association. Thus, higher association observed between PA200 and the s20S could be due to a higher PSMA8 gene expression in these cells.

Taken together, our IP strategy revealed that the s20S has an interactome distinct from that of the c20S. The s20S interactome we mapped here is enriched for the 19S particle, as well as different components of the UPS and synaptonemal proteins. The differences between the c20S and s20S interactomes suggest distinct functions of these proteasome variants.

Proteasome dynamics analysis throughout spermatogenesis

An important limitation of our whole testis analysis is the lack of information on the dynamic interactions that are frequently lost and/or rearranged upon tissue lysis (Wang and Huang, 2007), and information on proteasome dynamics throughout spermatogenesis. To provide a detailed map of the proteasome interactome during spermatogenesis, we initiated a study of individual germ cell populations. We harvested testes from young adult or pre-pubescent rats, and immediately dissected and digested them into individual cells. Rat germ cells were purified and separated either by sedimentation at unit gravity (SPG) or centrifugal elutriation (SPC and SPT), in order to obtain highly enriched cell populations. SER were also purified, since they are support cells of the germ cell lineage and might carry relevant information. Proteasome complexes from these purified fractions of cells were co-immunopurified using the antibody directed against the α2 proteasome subunit (Fabre *et al.*, 2015). Purified complexes were digested with trypsin and the resulting peptides analyzed on a nanoLC-MS/MS system, followed by protein identification and relative quantification. In parallel, lysates of individual groups of cells were directly analyzed without the IP step to obtain complementary information on protein expression and to validate the cell purification protocol. Among the 5750 proteins validated and quantified in the lysates using label-free MS, a pool of 12 proteins were unambiguously identified as specific markers of each cell type (**Supplementary Fig. S8**). Proteasome complexes immunopurified from the different groups of cells were then analyzed using the same approach to observe changes in 20S proteasome composition throughout spermatogenesis (**Fig. 3**). None of the three i20S catalytic subunits could be detected in the four different cell types studied, suggesting that the i20S subunits previously detected in the whole bovine testis sample are likely derived from infiltrated immune cells. Another striking observation was that the α4s isoform almost completely replaced α4 at the SPC and remained the main isoform throughout spermatogenesis (**Fig. 3A)**. This trend was also observed in cell lysates (**Fig. 3B**), and may be driven by changes in the expression of the two isoforms.

Our analysis of proteasome activators (19S, PA28αβ, PA28γ, and PA200) indicated that the 19S is the predominant regulator associated with the 20S particles, whatever the cell type analyzed, and was bound from around 30% (in SER and SPG) up to 60% (in SPC and SPT) of the total 20S pool (**Fig. 3C**). The fraction of 20S-19S complexes thus significantly increases 1.7-fold (*p-value* = 0.01) when SPG proceeds into the SPC stage (**Fig. 3D**), highlighting a high demand for cellular ubiquitin-dependent proteolysis. While the nuclear PA28γ activator levels do not significantly change through spermatogenesis, its cytoplasmic counterpart PA28αβ significantly decreased (7.2-fold) from the SPG to SPC stages (*p-value* = 0.005) (**Fig. 3D**). The abundance of PA200 bound to the 20S core particle increases 7.5-fold in SPC (*p-value* = 0.002) and 6.6-fold in SPT (*p-value* = 0.01) compared to SPG, in agreement with the proposed role of PA200 in spermatogenesis (Khor *et al.*, 2006) (Qian *et al.*, 2013). Here, increase in proteasome bound PA200 appears to be mainly the consequence of increased expression (**Supplementary Fig. S9**), which is in accordance with the existing literature (Zhang *et al.*, 2021). However, given that we did not observe increased binding of PA200 to s20S in the whole testis interactome analysis, it remains difficult to draw conclusions about specific PA200 interactions. Concerning α4s, its increase in lysates from the SPG to SPC stages is approx. two-fold higher than its increase in immunopurified proteasomes (*p-value* = 0.007, **Supplementary Fig.S9**). This may be due to a chaperone-mediated resistance to α4s incorporation into functional 20S proteasomes, or to the lag time between synthesis of α4sand its incorporation in newly-assembled s20S. Increase in the association of 19S and PI31 with 20S proteasomes from SPG to SPC is, to a certain extent but not completely, explained by higher cellular abundances, since their increase in the immunopurified proteasomes are significantly higher than in full lysates (FC = 1.4 and 2.7; *p-value* = 0.03 and 0.006, respectively, **Supplementary Fig.S9**). Given that 20S-associated regulators display different substrate specificities and subcellular localization (Stadtmueller and Hill, 2011), the observed variations in the panel of proteasome activators suggest profound changes in the biological function and/or subcellular localization of proteasomes throughout spermatogenesis.

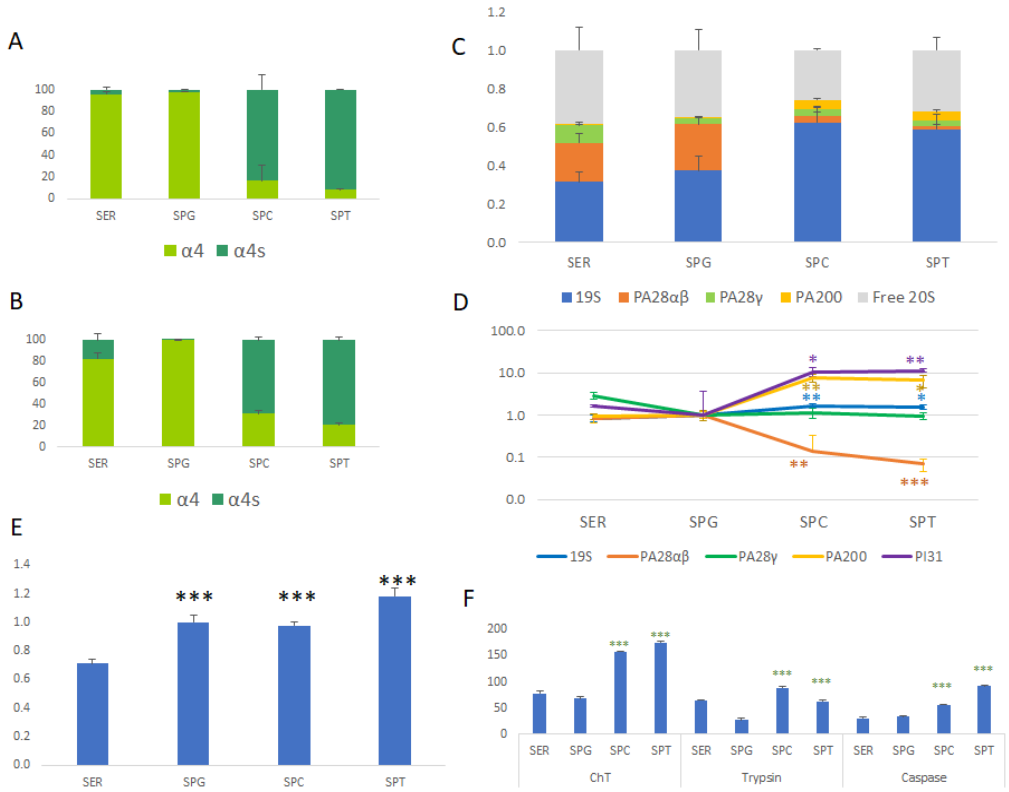

Figure 3. Composition and proteolytic activity of proteasome complexes purified from rat Sertoli cells (SER), Spermatogonia (SPG), Spermatocytes (SPC) and Spermatids (SPT). Cells obtained from rat testes were separated and then analyzed using label free proteomics. **(A-B)** Proportions of α4 and α4s proteins in **(A)** immunopurified proteasome complexes and **(B)** cell lysates. **(C)** The distribution of the different proteasome complexes was estimated for each cell type by label-free MS (Fabre *et al.*, 2014). We considered the free 20S complexes and the ones associated with 19S, PA28αβ, PA28γ, and PA200 regulators. Error bars indicate standard deviation across three biological replicates. **(D)** Major changes in the composition of proteasome complexes throughout spermatogenesis. The variations of major 20S-associated regulators were measured throughout spermatogenesis using label-free quantitative proteomics. The SPG stage was used as a reference and stars indicate significance between SPC *vs.* SPG or SPT *vs.* SPG. **(E)** Changes in the amount of total 20S proteasomes throughout spermatogenesis. The variations of 20S proteasome subunits (all non-catalytic subunits except α4 and α4s) were measured throughout spermatogenesis using label-free quantitative proteomics and normalized with the MS signal of total protein. Stars indicate significance between SPG *vs.* SER or SPC *vs.* SER or SPT *vs.* SER. **(F)** Proteasome chymotrypsin-like (ChT), trypsin-like and caspase-like specific activities, expressed in pmol AMC released per minute and per mg of total protein, have been measured in the four cell types lysates throughout spermatogenesis. Stars indicate significance between SPC *vs.* SPG or SPT *vs.* SPG. **All panels**: Graphics represent mean and standard deviations. All values are the means of three independent experiments. * : $p<0.05$; **: $p<0.01$; ***: $p<0.001$.

Overall, a large proportion of the 20S proteasome pool was bound to activators, reaching almost 75% in SPC cells, which represents a specific feature of testis cells as

the proportion of activated 20S core is usually around 20 to 60% in other tissues (Fabre *et al.*, 2014). Moreover, all three germ cell types contain slightly but significantly higher amounts of total 20S compared to SER (**Fig. 3E**). Chymotrypsin, trypsin, and caspase-like proteolytic activities were significantly higher in meiotic and post-meiotic germ cells (SPC & SPT) compared to undifferentiated SPG (**Fig. 3F**), which is most probably the consequence of two major events, *i.e.* the complete replacement of α4 by α4s isoform and the increase in activator-associated 20S, in particular the higher loading of 19S and PA200 particles.

We also noted that PI31 has a dramatic increase (11-fold) in 20S core particle association in both SPC and SPT stages, compared to non-differentiated SPG cells (*p-values* of 2E-03 and 8E-04, respectively) (**Fig. 3D**). Accordingly, its known interactor Fbxo7 was only detected in proteasome complexes purified from SPC and SPT. No significant variation of 20S-associated regulators can be observed from SER to SPG cells which also display similar 20S proteasome composition, in particular their high content of α4. The observed variations in proteasome proteolytic activities and 20S-associated regulators in pre-meiotic (SPG) *vs.* meiotic and post-meiotic cell types (SPC & SPT) thus suggest either a possible increased ability of the s20S to interact with its activators, compared to the c20S, or a transcriptionally-driven increase in the quantities of these regulators in post-meiotic stages. To answer this crucial question, we analyzed variations of expression of these different proteins in the different cell lysates. Changes from SPG (containing exclusively c20S) to SPC and SPT (containing 85-90% s20S, **Fig. 3A**) were thus compared both in the immunopurified proteasome samples and in the lysates (**Supplementary Fig. S9**). Altogether this dataset indicates that changes in the composition and activation of 20S proteasomes from the SPC stage onwards may, at least partly, result from transcriptional regulation; however, at this stage we can't exclude the possibility that other mechanisms and factors may be involved.

Pull-Down assays show a preferential binding of the s20S to the 19S

In order to examine preferential interactions between α4s and PI31, 19S and PA200 (compared to α4), we took advantage of the testes 20S pool immunopurified in mg quantities from bovine testes. After incubation of these three partners of the 20S with either pure c20S (purified from bovine muscle) or the testes 20S pool (purified from bovine testes), we pulled-down complexes using anti-PI31, anti-19S or anti-PA200 antibodies-grafted beads, and estimated the relative amounts of α4 and α4s in the eluates using LC-MS/MS label free quantification. A control pull-down was run concurrently with the MCP21 antibody that equally recognizes the c20S and s20S. After normalization of the signal with the MCP21 IP, we found that PI31 was interacting more with proteasomes with α4 than with α4s **(Fig. 4A)** (*p-value* = 0.018). However, the 19S pull-down (anti-PSMC2) was much more efficient in co-purifying α4s than α4 (*p-value* = 0.0002) **(Fig. 4B)**. Finally, the

anti-PA200 IP showed no significant difference between α4 and α4s pulldowns **(Fig. 4C)**. Altogether, these *in vitro* binary interaction experiments suggest that the c20S and s20S preferentially interact with PI31 and the 19S, respectively; while there is no clear evidence that PA200 interacts preferentially for any of these 20S subtypes.

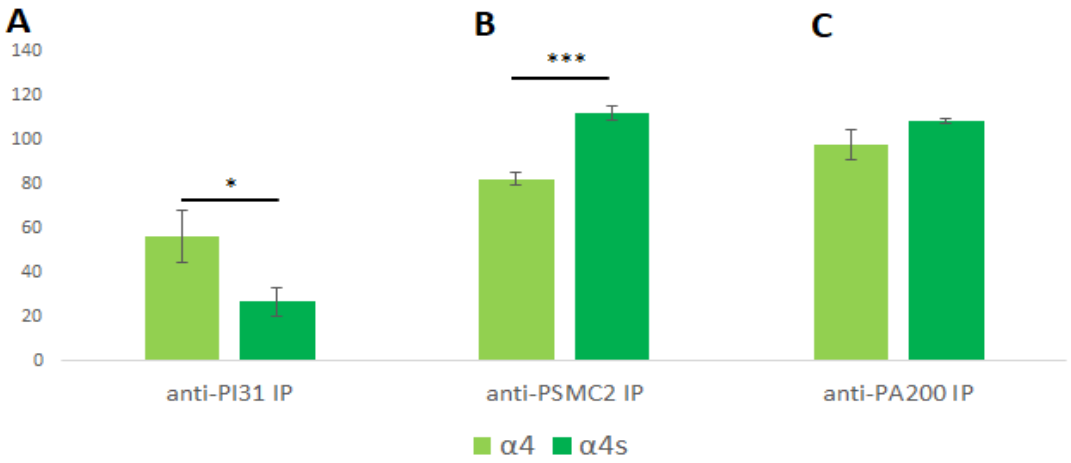

Figure 4. In vitro pull-down assays. Bovine c20S or testes 20S pool were incubated with **(A)** PI31, **(B)** the 19S or **(C)** PA200, and complexes were purified with sepharose beads grafted with their corresponding antibodies. After washes and elution, α4 and α4s subunits were identified and quantified by LC MS/MS label-free quantification and their abundances in anti-PI31 IP, anti-PSMC2 IP, and anti-PA200 IP were normalized with their abundances in the corresponding control IPs. Anti- α2 subunit control IP (for total 20S) was performed on the same reaction mix for each experiment. Graphics represent mean and standard deviations. All values are the means of three independent experiments. Stars indicate significance * : $p<0.05$; **: $p<0.01$; ***: $p<0.001$. The vertical axis represents the intensity of a protein in a pull-down experiment relative to its intensity in a control IP (in the case of 19S - average intensity of a set of 19S base proteins), when normalized for 20S abundance.

HDX-MS rationalizes the spermatoproteasome structural singularity

We recently implemented HDX-MS, a technique which reports on solvent accessibility and/or flexibility of the backbone amide protons, on the c20S and i20S proteasome complexes, in order to decipher their structural rearrangements upon replacement of their catalytic subunits and binding to PA28 regulators (Lesne *et al.*, 2020). Building on this expertise, we investigated the conformational differences due to the replacement of α4 by α4s. The relatively large amount (~180 µg per condition) of pure 20S required to perform such structural studies led us to use the testes 20S pool purified from bovine testes. This prevented us from comparing the deuteration of any peptides common to the c20S and s20S. However, 33 and 27 of the 53 and 47 peptides obtained upon pepsin digestion of α4 and α4s, respectively, were proteospecific (**Supplementary**

Fig.S10). We manually compared the deuteration heatmaps obtained for both α4 and α4s after alignment (**Fig. 5A**) and clearly identified two regions, encompassing residues 180-189 and 225-250, that were more readily deuterated in α4s compared to α4 (**Fig. 5A-C**). Interestingly, these two regions face each other on the outer surface of the α-ring, based on the c20S structure (**Fig. 5B**). To explore possible impacts of these differences on structure and dynamics of α4 and α4s, we employed 1 µs all-atom molecular dynamics simulations. We could detect ~64% more hydrogen bonds (H-bonds) between the NH groups of the backbone and water molecules for α4s than for α4 (**Fig. 6A**) in line with our HDX-MS results. Furthermore, the distribution of the crossing angle between the two last α-helices was broader in α4s compared to α4 (**Fig. 6B,** standard deviation = 8.3° and 6.2° for α4s and α4, respectively), indicating that the motion between these two helices is more important in α4s. Looking in more detail, we observed that these two helices were stabilized by H-bonds between three pairs of side chain residues (E235/K193, E231/K189 and Y228/D185 for α4 and E235/R193, E231/K189 and Q228/N185 for α4s) (**Fig. 6C**). Interestingly, the frequency of these H-bonds was found much higher in α4 than in α4s, especially between residues 235 and 189 (**Fig. 6D and Supplementary Fig. S11A**), explaining the higher motion of these helices, the larger number of H-bonds between its backbone and water molecules and the overall faster deuteration in α4s. In line with these results, the average Accessible Surface Area (ASA) of residues 184-198 and 225-241 was higher in α4s than in α4 (**Supplementary Fig. S11B**). Altogether, our results indicate more dynamic movements of both 180-189 and 225-250 regions in the s20S compared to the c20S, potentially creating a different binding interface and resulting in the differences in the interactomes we mapped above.

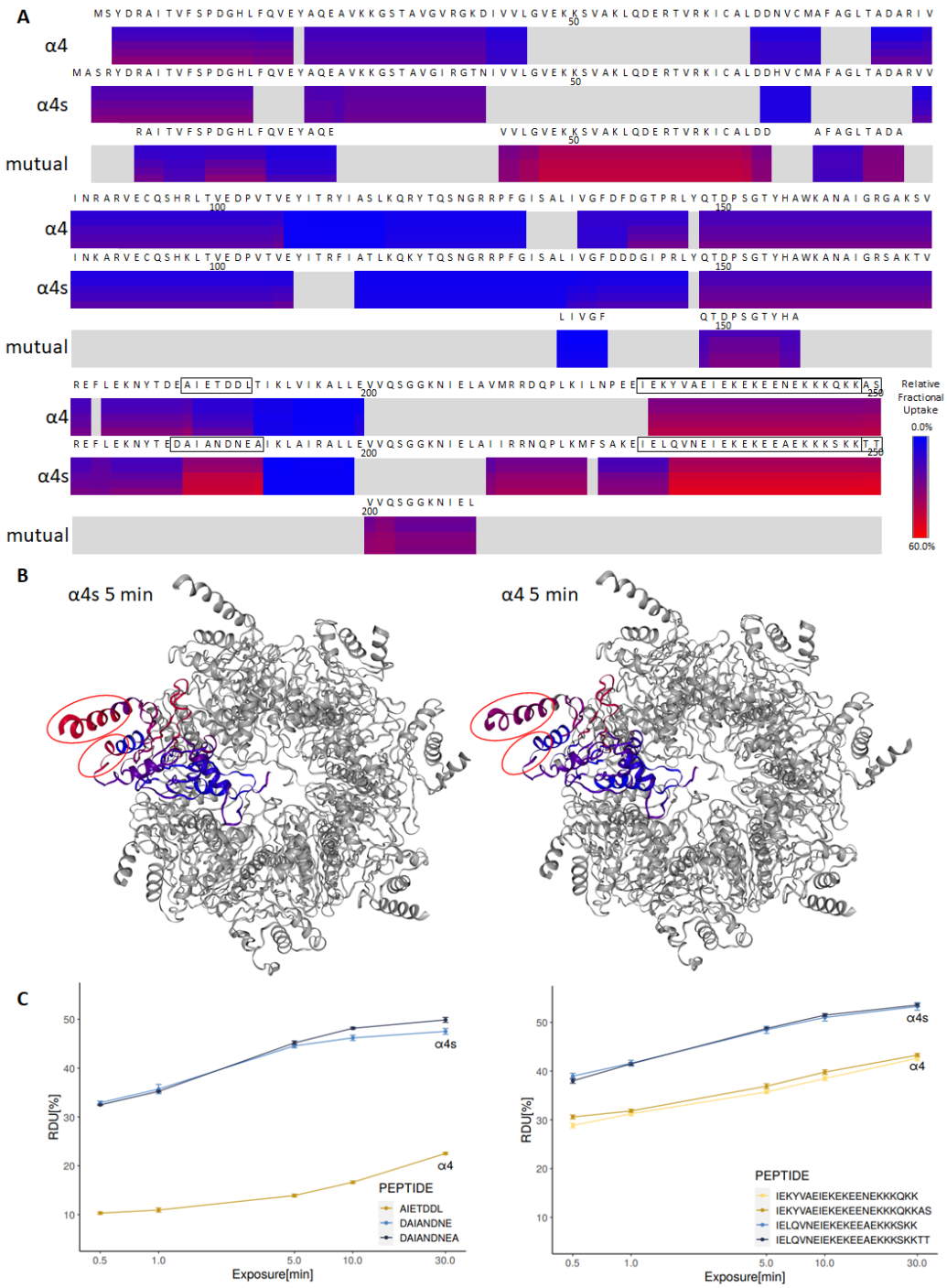

Figure 5. HDX-MS of the s20S *vs.* c20S. **(A)** Heatmap showing the relative deuterium uptake from 0% (blue) to 60% (red) of α4 and α4s at 0.5 min, 1 min, 5 min, 10 min and 30 min. **(B)** Cartoon representation of a homology model of α4s (left) and the structure of α4 (right) within the 20S bovine proteasome (PDB: 1IRU), viewed from the top of the α-ring. Residues of α4s and α4 are color coded with the relative deuterium uptake at 15 min. **(C)** Kinetics of deuteration obtained for 7 peptides of α4s or α4 encompassing residues 180-189 (left) and 225-250 (right), all showing a more limited deuteration of α4 compared to α4s.

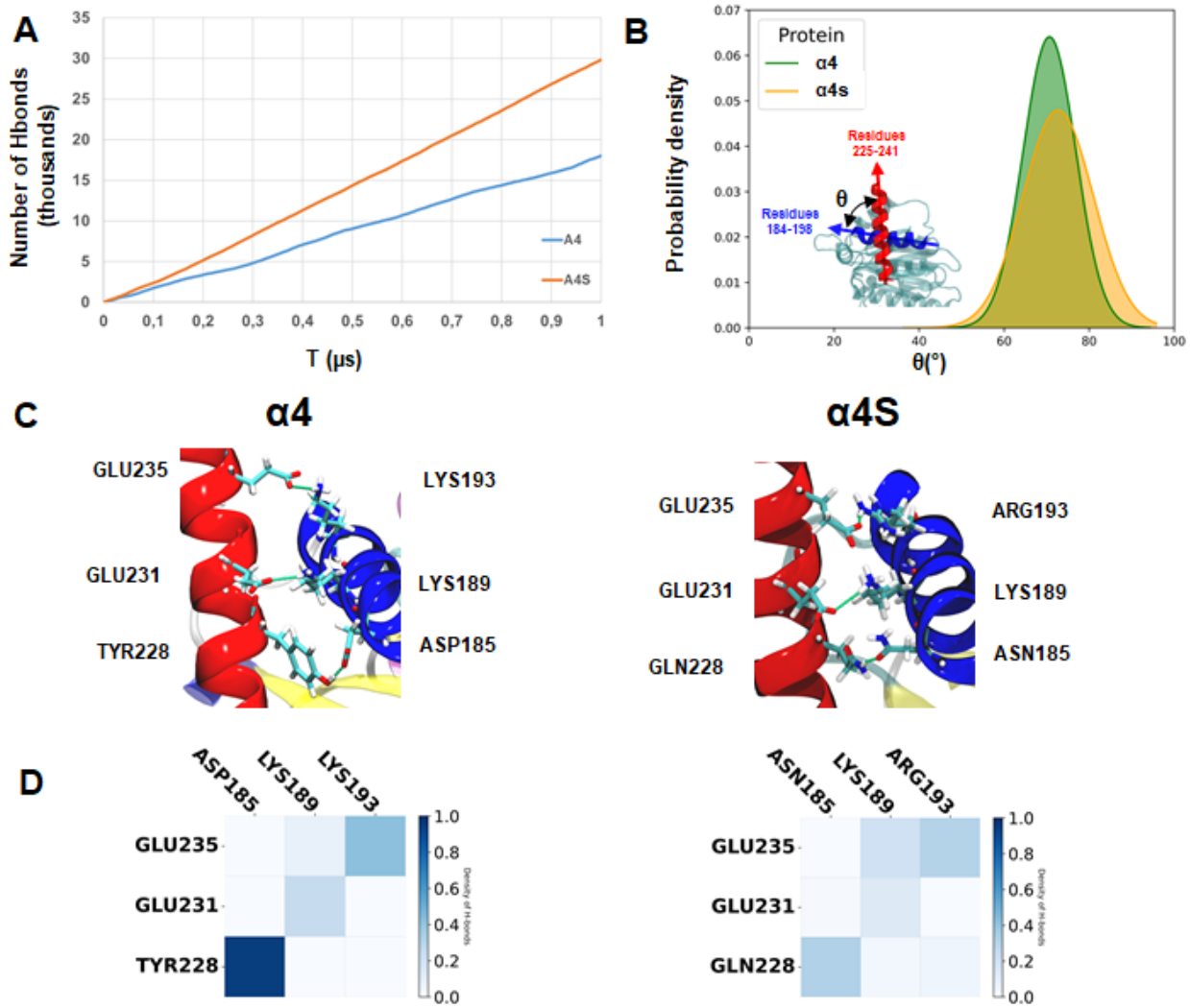

Figure 6. Molecular dynamics simulations of α4 and α4s. **(A)** Number of H-bonds observed for the amide protons of residues 184-198 and 225-241 of α4s (orange line) and α4 (blue line) during the 1 µs simulation. **(B)** Distribution of crossing angles between the two last α-helices of α4s (yellow) and α4 (green). **(C)** Close-up view of the two last α-helices of α4 (left) and α4s (right). **(D)** Normalised frequency of H-bonds observed between the side-chain residues of the two last α-helices of α4 (left) and α4s (right).

Testis and muscle proteasomes show distinct peptidase activities

We tested whether α4s incorporation into the 20S core induces any change in proteasome activity on its, own or in complex with a regulator. We compared the testes 20S pool purified from bovine testes, which contains approximately 50% of s20S, and the c20S purified from bovine muscle in their ability to degrade fluorogenic substrates. The substrates assayed were suc-LLVY-AMC, boc-LRR-AMC and z-LLE-AMC, which probe the chymotrypsin-like, trypsin-like and caspase-like activity, respectively. The two proteasome samples were also activated with two different ratios of 20S to PA200

regulator. When comparing the basal activity of the proteasome, the s20S mix showed significantly greater trypsin- and chymotrypsin-like activity, while the caspase-like activity was more or less the same (**Fig. 7**). The addition of PA200 did activate the 20S proteasomes in both cases, with more pronounced activation achieved with 1:8 molar ratio of 20S to PA200. Although trypsin-like activity change upon PA200 binding is greater in c20S, the overall tryptic activation of the complex remains significantly greater in the s20S. In both molar ratios tested, the activated complex's chymotrypsin-like activity is also greater in the s20S. The activation of the caspase-like activity is somewhat more pronounced in the c20S compared to the s20S. Overall, these results show that s20S seems to have higher trypsin and chymotrypsin-like activities than c20S, both at basal state and when activated with PA200.

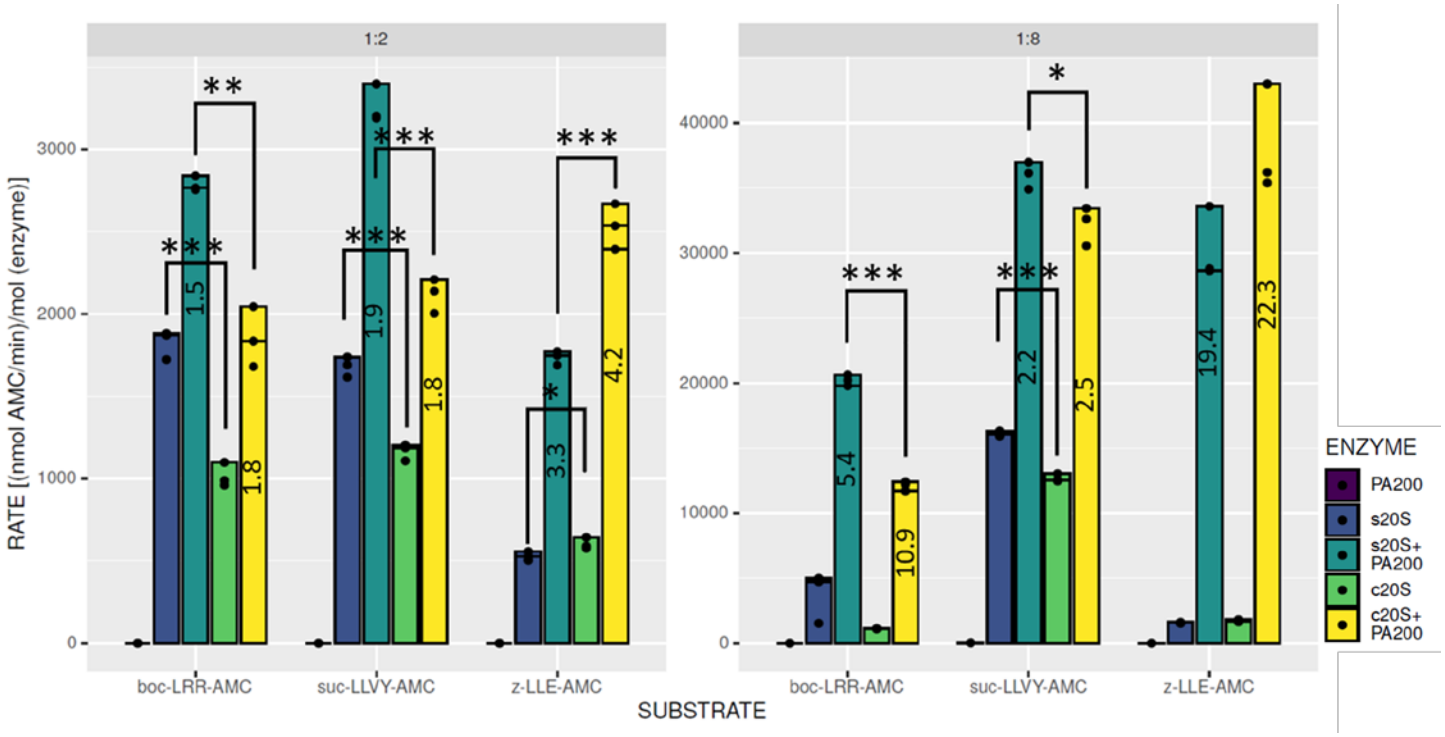

Figure 7. Comparison of three peptidase activities in proteasomes purified from bovine testis or muscle, presented by overlaid dot plots and box plots. Activation of the proteasomes by PA200 was assayed in two different molar ratios, separated in the left (1:2) and right (1:8) panel with separate vertical axes. The bars are grouped by the peptide used to probe each activity: suc-LLVY-AMC, boc-LRR-AMC and z-LLE-AMC, which probe the chymotrypsin-, trypsin- and caspase-like activities, respectively. The numbers on some bars represent the fold-change activation of a 20S-PA200 complex compared to the 20S complex of the same type (always first on the left). Different complexes are represented by different colours. PA200 alone was tested as a control, and showed no fluorescence change over time. All values are the means of three independent experiments. Stars indicate significance. * : $p<0.05$; **: $p<0.01$; ***: $p<0.001$.

Discussion

Despite being recognized as important for mammalian male germ cell differentiation and spermatogenesis, the testis-specific proteasome isoform s20S remains incompletely characterized. Here, we combined state-of-the-art MS-based proteomic analyses with *in vitro* studies to conduct a comparison between s20S and c20S, using α4s and α4 as markers for each proteasome variant, respectively. We found that α4s represents ~42-45% of all α4 variants found in whole bovine testis, suggesting that the s20S is a major proteasome form in testicular tissue. We also showed that α4 and α4s do not co-exist within assembled proteasomes, in line with immunofluorescence imaging experiments (Zhang *et al.*, 2019). This exclusive incorporation of α4 or α4s subunits into proteasomes may be either due to a selective subunit incorporation or to a sudden change in protein expression levels. To address this question, as well as map dynamic proteasome changes that accompany spermatogenesis, we analyzed isolated populations of rat germ cells at different differentiation stages (SPG, SPC, SPT) and their supportive cells (SER). This demonstrated that SPG 20S proteasomes contained almost exclusively α4 (>98%), whereas pachytene SPC and SPT predominantly had α4s-containing proteasomes (>82%-92% α4s). This sudden change in the abundance of α4s vs. α4 may be driven by rapid changes in transcription resulting in major differences in protein levels.

The shift of c20S to s20S observed from pre-meiotic SPG to meiotic SPC was accompanied by profound changes in the major 20S-associated regulators, in particular an increase in PA200 and 19S activators, concomitantly with a decrease in PA28αβ and related 20S immunocatalytic subunits. Surprisingly, no change in PA28γ could be observed, although this 20S activator was previously shown to be relevant to male fertility (Huang *et al.*, 2016; Gao *et al.*, 2019). It has been recently proposed that PA200 constitutes a major component of the s20S complex (Qian *et al.*, 2013; Zhang *et al.*, 2021) and that α4s may help the formation of PA200-capped complexes containing only standard catalytic subunits (Zhang *et al.*, 2021). Accordingly, our results indicate that PA200 is an important player in s20S function, as its level of incorporation into assembled proteasomes in SPC and SPT (around 8-10%) is at least 10-fold higher than previously measured for several other cell types (Fabre *et al.*, 2014). We also show that the 19S is the major activator of 20S core particles in germ cells, and is found binding to around 30-40% of the total 20S pool in SER and undifferentiated germ cells. Strikingly, the proportion of proteasomes bound to 19S in SPC and SPT cells increases up to 60%, making meiotic and post-meiotic proteasomes highly activated. This agrees with the increased proteolytic activities in SPC and SPT, compared to SPG and SER, and similar previous observations using whole testis lysate compared to muscle tissue (Qian *et al.*, 2013). Another study also showed high levels of 19S-containing species in post-meiotic germ cells (Gomez-H *et al.*, 2019) and in whole testes (Qian *et al.*, 2013; Zhang *et al.*, 2021). The increased

association between s20S and activators during spermatogenesis is aligned with increased proteolytic requirements of this process.

We observed that PI31, previously described as a 20S proteasome inhibitor (Li *et al.*, 2014) and a 26S proteasome activator (Bader *et al.*, 2011), and its binding partner Fbxo7 (Kirk *et al.*, 2008) were both enriched in the s20S samples. This agrees with earlier observations in *Drosophila* and mice spermatogenesis (Bader *et al.*, 2011; Rathje *et al.*, 2019). Furthermore, PI31 was shown to mediate proteasome transport in axons and dendrites in mice, by regulating the loading of proteasomes onto microtubule-dependent molecular motors (Liu *et al.*, 2019). Accordingly, here we identified several microtubule-related proteins interacting with the s20S, which could facilitate such transport of s20S complexes. On the other hand, as a part of its E3 ligase activity, Fbxo7 targets proteins involved in cell cycle regulation (Meziane *et al.*, 2011). Thus, we speculate that PI31 and Fbxo7 might act as shuttle proteins for the s20S, targeting cyclins and other spermatogenesis-specific substrates; however, mechanistic details of s20S-PI31-Fbox7 remain to be established.

Another class of s20S-specific interaction partners we identified are SYCE1 and SYCP3, components of synaptonemal complexes. These findings further support the proposed mechanism whereby s20S binds to the synapses along the axes of the meiotic chromosomes, to regulate this process through the degradation of specific proteins (Gomez-H *et al.*, 2019) (Prasada Rao *et al.*, 2017). Although previous work suggested that SYCP3 was a substrate of the s20S (Gomez-H *et al.*, 2019; Prasada Rao *et al.*, 2017), our data indicate high sequence coverages of SYCP3 and SYCE1 in our interactome study (25% and 34%, with 4 and 9 peptides, respectively), which is typical of true interactors. Moreover, recent work on s20S KO mouse models did not replicate the SYCP3 accumulation (Zhang *et al.*, 2019), further strengthening the argument for SYCP3 as a s20S interactor. Taken together, our quantitative interactome data indicate extensive differences between c20S and s20S, and show that spermatogenesis is accompanied by a major shift from c20S as the major proteolytic machinery towards s20S.

Given that the only difference between c20S and s20S is the presence of α4 or α4s isoforms, we employed HDX-MS to examine whether they display any differences in structure and dynamics. Our analysis revealed pronounced differences in flexibility of the C-terminal regions of the two isoforms, corresponding to the two last α-helices located on the outer, solvent-exposed side of both α4 and α4s structures. Our HDX-MS data showed that these two helices are more rigid (or stabilized) in α4 than in α4s. Molecular dynamics simulations provide a rationale for these observations, by predicting more stable hydrogen bonds between the two C-terminal helices in α4. In order to understand functional consequences of these differences, we performed pull-down assays with α4- and α4s-containing proteasome and immobilized proteasome regulators, PI31, PA200

and 19S. We observed differences in pull-down efficiency for PI31, which showed significantly greater affinity towards the α4-containing proteasome (c20S), and 19S, which had a higher affinity towards the s20S. However, we did not observe any differences in affinity of PA200. Finally, we also tested proteolytic activity of proteasomes purified from bovine testes (~50% s20S) and from the muscle (100% c20S) in two different conditions: alone and when activated by PA200. We measured that s20S has higher basal trypsin- and chymotrypsin-like activity, and this trend held upon PA200 activation. On the other hand, caspase-like activity for 20S alone was either the same or very similar, while the c20S-PA200 complex was more active than the s20S-PA200. Interestingly, upon PA200 binding, the fold-change in caspase-like activity is the most pronounced, confirming previous observations (Blickwedehl *et al.*, 2008). Increased basal level of tryptic activity can lead to improved degradation of substrates that are highly positively charged, such as histones, in agreement with the report that showed histones to be the targets of the PA200-20S complex in the context of spermatogenesis (Qian *et al.*, 2013). Overall, these activity measurements indicate significant difference in behavior of the α4s-containing proteasome, compared to the α4-containing proteasome.

Taken together, the large amount of data analyzed and presented in the context of this study highlight some key differences between c20S and s20S. Our results imply a more complex process of s20S regulation than previously suggested and underlies the functional differences between the s20S and c20S proteasome variants.

Material and methods

Proteome Repository Search

For data on relative expression at the protein level of the proteasome and proteasome-related genes we searched The Human Proteome Map portal by querying the list of relevant genes. The portal was described in (Kim *et al*., 2014).

Reagents

Unless stated otherwise, all reagents were purchased from Euromedex. The c20S, i20S, PA28γ and PA28αβ were purchased from Enzo Life Science.

The mouse IgG1 anti-α2 antibody was produced from the hybridoma cell line MCP21 (European Collection of Cell Cultures).

Antibody development

Anti-α4s antibodies were produced by Biotem (Apprieu, France). Two peptides were synthesized, C+ILNPEEIEKYVAEIEKEKEENEKKKQKKAS - corresponding to the α4-specific C-terminal sequence (P1 peptide) and C+MFSAKEIELQVNEIEKEKEEAEKKKSKKTT - corresponding to the α4s-specific C-terminal sequence (P2 peptide). Two New Zealand White rabbits, 20 to, 25 weeks old,

were immunized with a KLH-P2 conjugate (Day 0), by subcutaneous injection containing incomplete Freund's adjuvant. Immunisations were repeated on Day 7, Day 14 and Day 35. The rabbits were exsanguinated on Day 42 after the immunisation and the antibodies were affinity-purified from the blood serum using the immobilized P1 peptide, followed by depletion step using immobilized P2 peptide, in order to remove the α4-reactive antibodies. The obtained anti-α4s polyclonal antibodies exhibited an EC50 of 0.005 µg/mL against the α4s epitope and of 2.12 µg/mL against its α4 counterpart (**Supplementary Fig.S4B**). Moreover, the specificity of the newly-produced anti-α4s antibody was verified by western-blot assay (**Supplementary Fig.S4C**).

Proteasome Purification

Eight mg of MCP21 antibody was grafted to one gram of CNBr-activated Sepharose beads. Frozen bovine testis (-80 °C) from an adult individual were broken into pieces using a hammer and chisel. Lysis and coIP were then done at 4 °C. Ten grams of tissue were diced and placed into a blender with the lysis buffer (20 mM Tris HCl, 0.25% TritonX-100, 100 mM NaCl, 10 mM ATP, 5 mM MgCl2, 1 tablet of inhibitors/50 mL (cOmplete™ ULTRA Tablets Mini EDTA-free, Merck, Darmstadt, Germany), pH 7.6), at 1.6 weight to volume ratio. The lysate was passed through a Dounce homogenizer and then sonicated in a VibraCell (Bioblock Scientific, France) (power = 2, 60% active cycle, 10 cycles, 30 sec per cycle). The lysates were centrifuged for 30 min at 4 °C, 4500 g and the greasy supernatant was aspirated from the top of the lysate. The solid pellet was also discarded while the remaining liquid was again centrifuged at 4 °C and 16000 g , for 30 min. The supernatant was filtered through a 0.22 µm membrane. The filtered lysate was then mixed with the Sepharose grafted with antibodies and incubated at 4°C overnight. The next day, the Sepharose was washed with 50 mL of Equilibration buffer (20 mM Tris HCl, 1 mM EDTA, 10% glycerol, 100 mM NaCl, pH 7.6) and eluted with Equilibration buffer supplemented with 3 M NaCl. The eluate was concentrated on Amicon filters of 100 kDa cutoff (Millipore) and separated using gel filtration chromatography. The chromatography was performed on a Superose 6 10/300 GL column, using TSDG buffer (10 mM Tris-HCl pH 7.0, 1 M KCl, 10 mM NaCl, 5.5 mM MgCl2, 0.1 mM EDTA, 1 mM DTT, 10% Glycerol). The fractions were assayed by SDS-PAGE and 20S proteasome fractions were pooled together.

Preparation of separated germ cells from rats

Spermatogonia (SPG) were isolated from testes obtained from thirty 8-day-old Sprague Dawley (SD) rat testes with a purity of greater than 90% as previously described (Com *et al.*, 2003). Seminiferous epithelial cells were dispersed by enzyme treatment and separated. Briefly, the cells were separated by sedimentation velocity at unit gravity at 4 °C, using a 2–4% BSA gradient in Ham'F12/DMEM in an SP-120 chamber (STAPUT). After 2.5 h of sedimentation, 35 fractions were collected. Cell fractions 16 to 21 were pooled, washed 3 times with Phosphate Buffered Saline pH 7.4 and cells were

immediately subjected to in vivo cross-linking to stabilize proteasome interactors, as previously described (Fabre *et al.*, 2013). Cross-linked cells were stored at -80°C.

Pachytene spermatocytes (SPC) and early spermatids (SPT) were isolated from testes obtained from eight 90-day-old SD rat and prepared by centrifugal elutriation with a purity greater than 90% according to a previously described method (Pineau *et al.*, 1993), except that enzymatic dissociation of cells was replaced by mechanical dispersion. Upon isolation, cells were washed 3 times with Phosphate Buffered Saline pH 7.4 and cells were immediately subjected to in vivo cross-linking as previously described (Fabre *et al.*, 2013). Cross-linked cells were stored at -80°C.

Sertoli cells (SER) were isolated from testes obtained from eight 20-day-old SD rats according to previously described methods (Skinner and Fritz, 1985; Toebosch *et al.*, 1989). The cell suspensions were seeded at a density of approximately 1x10^6 cells/mL in 75 cm2 tissue culture flasks (NUNC, Copenhagen, Den- mark). The cells were then incubated at 32°C in a humidified atmosphere of 5% CO2 and 95% air in Ham's F12/ DMEM supplemented with insulin (10 mg/mL), Human transferrin (5 mg/mL) and gentamycin (10 mg/mL), all from Life Technologies (Eragny, France). Culture medium was changed daily until the end of the experiment. On the second day of culture, the cells were exposed to a hypotonic treatment in order to eliminate the contaminating germ cells. The degree of purity of the isolated Sertoli cells was > 98%. On day 5 of culture, cells were recovered, washed 3 times with Phosphate Buffered Saline pH 7.4 and were immediately subjected to in vivo cross-linking as previously described (Fabre *et al.*, 2013). Cross-linked cells were stored at -80°C.

<u>Proteasome immunopurification from rat germ cells and sample preparation for LC-MS</u>

Immunopurification of proteasome complexes from rat germs cells was done using the MCP21 clone of the anti-α2 antibody and sample preparation was done by in-gel digestion, as described in (Bousquet-Dubouch *et al.*, 2009). For this protocol, pools of cells from different rats, 8-10x10^6 SER, 20-25x10^6 of SPGs, 8x10^6 of SPCs and 20x10^6 of SPTs per replicate were used. Three independent experiments were run for each type of cell.

<u>Co-immunopurification for interactomics from bovine testis and sample preparation for LC-MS/MS</u>

Four biological replicates of frozen bovine testes (-80 °C) from adult individuals were broken into pieces using a hammer and chisel. Lysis and coIP were then done at 4 °C. Ten grams of tissue were diced and placed into a blender with the lysis buffer (20 mM Tris HCl, 0.25% TritonX-100, 100 mM NaCl, 10 mM ATP, 5 mM MgCl2, 1 tablet of protease inhibitors/50 mL (cOmplete™ ULTRA Tablets Mini EDTA-free, Merck, Darmstadt, Germany), pH 7.6), 1.6 weight to volume ratio. The lysate was passed through a Dounce homogenizer and then sonicated in a VibraCell (Bioblock Scientific, France)

(power=2, 60% active cycle, 10 cycles, 30 sec per cycle). The lysates were centrifuged for 30 min at 4 °C, 4500 g and the greasy supernatant was aspirated from the top of the lysate. The solid pellet was also discarded while the remaining liquid was again centrifuged at 4°C and 16,000 g , for 30 min. The supernatant was filtered through a 0.22 µm membrane. The co-immunopurification of the proteasome complexes was done using ProteinG coupled to the magnetic beads (MagBeads, Cat. No. L00274, GenScript USA Inc. Piscataway, NJ USA). The protocol proposed by the supplier was followed with the following modifications. The amount of beads used per sample was 100 µL of suspension. The amount of antibodies used per replicate was 100 µg of anti-α4s, 50 µg of anti-α2, 10 µg of anti-PA200 and 50 µg of OX8 control antibody. One mL of lysate of each replicate was incubated with ProteinG-MagBeads, coupled with different antibodies, overnight at 4 °C on a rocker. Samples were then washed four times with Equilibration buffer (20 mM Tris HCl, 1 mM EDTA, 10% glycerol, 100 mM NaCl, 2 mM ATP, 5 mM MgCl2, pH 7.6), then eluted with 25 µL of S-trap Elution Buffer (5% SDS, 50 mM TEAB, pH 7.55). In case of anti-α4s, proteasome complexes were eluted via competitive elution method, for improved signal/noise ratio. Namely, the peptide used for immunization of the animals and production of antibody was used to elute the antibody from the MagBeads. Peptide was diluted in the Equilibration Buffer to 160µg/mL and 100µL of the peptide solution were added per replicate. The beads were incubated for 1h at room temperature, while mixing. The supernatant was recovered and mixed with SDS solution to final 5% SDS. Control IP was also done with the OX8 control antibody and the peptide elution procedure.

Preparation for LC-MS analysis was done using S-trap micro cartridges (Protifi, Farmingdale NY USA), by default protocol of the manufacturer. Around 2 µg of peptides per sample per run were used for LC-MS analysis.

Bottom-up LC-MSMS

Analysis was performed on an Orbitrap Fusion instrument, with nano ESI source, coupled to the Ultimate 3000 chromatography system using 90 min runs, as described previously (Kelstrup *et al.*, 2018). Peptides were loaded onto a precolumn and washed (97.95% water, 2% ACN,0.05% trifluoroacetic acid). Upon loading onto the column (made in-house, 75µm ID, 50cm column, packed with Reprosil C18, 3 µm phase, Cluzeau), the elution gradient is initiated at 300 µL/min, by 100% phase A (0.2% formic acid) for 3min, then a slope 10-30% phase B (80% acetonitrile, 0.2% formic acid) for 50min, followed by 30-45% B gradient for 10min, to finish with 45-80% B during 1min. The 80% B was maintained for 10 to wash the column, followed by re-equilibration with the 100% phase A during 15min. The nano- ion source was at +1900 V, with ion transfer tube temperature at 275 °C. MS analysis was done in the Orbitrap at 60k resolution, scan range between 350 and 1400 m/z, with RF lens value set to 60%, AGC target set to 4e5, maximum injection time to 50 ms, with 1 microscan performed in profile mode. MSMS was done in data-dependant mode, in the Orbitrap, at resolution of 15k (first mass at 100 m/z). Monoisotopic peak determination was set for peptides, intensity threshold of 2.5e4 was used and only charge states from 2 to 6 were used as precursors. Dynamic exclusion

was used with the following parameters: exclude the ion after “1” times, during 30 sec, including isotopes, with mass tolerance, high and low, 10 ppm each. Ion isolation was done in the quadrupole, with an isolation window of 1.7 m/z. The activation was done by HCD at 28% collision energy. AGC was set to 5e4, ions were injected for all available parallelizable time, with maximum injection time of 22 ms. A total of 1 microscans per cycle was used and recorded in centroid mode.

Bottom-Up data treatment

Identification and quantitation parameters. The identification was done with Mascot search engine, using following search parameters: Peptide mass tolerance : 10 ppm; Peptide charge : 2+ and 3+; Cleavage enzyme: Trypsin/P; Max. missed cleavages : 2; Decoy : true; Mass : Monoisotopic; Fixed modifications : Carbamidomethyl (C); Variable modifications : Acetyl (Protein N-term),Oxidation (M); MS/MS IONS SEARCH : true; Error tolerant : false; MS/MS tolerance : 20 mmu; Data format : Mascot generic; Quantitation : None; Instrument : ESI FTMS HCD. The UniProt entries (SwissProt & TrEMBL) for *Bos Taurus* were used as a protein entry database, including isoforms. In the case of rat germ cells, the search was performed with *Rattus norvegicus* Uniprot database, including isoforms.

The result files were then imported into Proline – software for Bottom-Up proteomics (Bouyssié *et al.*, 2020), using following parameters: Peaklist software: Proline; Generate intermediate mzIdentML file: false; Instrument configuration: ORBITRAP FUSION (A1=FTMS F=HCD A2=FTMS); Decoy strategy: Concatenated Decoy Database; Protein match decoy rule: SearchGUI REVERSED; Ion score cutoff: None; Subset threshold: None; Replace peptide matches scores by PEP values (Posterior Error Probabilities): false; Automatically associate raw files to identification results (DAT, OMX): true. Validation of the peptide IDs in Proline was done using following parameters: PSM filters: Pretty Rank: 1.0, Peptide Seq Length: 7.0; PSM validation: expecting FDR of 1.0% on Mascot Adjusted E-Value; Validation of the protein sets was done using the following parameters: Min. specific peptide count: 1; Enable protein FDR (false discovery rate) filter: true; Min protein set FDR (%): 1.0; Peptide set scoring method: Mascot Modified MudPIT; Dataset merging mode: After validation (merge identification summaries). Label-free quantitation was done using following parameters: Quantitation type: label_free; Quantitation method: Label free based on the extraction of feature abundance; Extraction m/z tolerance: 5 ppm; Mapping m/z tolerance: 5 ppm; Min. peakel duration: 15 sec; Alignment computation method: (Iterative; Max number of iterations: 3; m/z tolerance: 5 ppm; Time tolerance: 5 sec); Alignment smoothing: (Method: Landmark Range; Number of landmarks: 50; Sliding window overlap: 50); Features cross assignment: (Mapping m/z tolerance: 5 ppm; Time tolerance: 60 sec; Normalization method: None; Master feature filter type: Intensity; Intensity threshold: 0). Normalization and statistics were done using the following parameters: Global options: (Apply profile clustering: false (method: QUANT_PROFILE); Use only specific peptides: true; Discard miscleaved peptides: false (method: KEEP_MOST_ABUNDANT_FORM); Discard oxidized peptides: false (method:

KEEP_MOST_ABUNDANT_FORM); Abundance summarizer method: LFQ based on QUANT_PEPTIDE_IONS); Protein options: (Apply normalization: true; Apply missing values inference: false; Apply variance correction: false; Apply T-test: true (p-value: 0.01); Apply Z-test: true (p-value: 0.4)); Peptide options: (Apply normalization: true; Apply missing values inference: false; Apply variance correction: false; Apply T-test: true (p-value: 0.01); Apply Z-test: true (p-value: 0.4)). The p-value for a non-paired, one-sided T-test and fold change were calculated between the experimental IP groups and the control IP groups (IP with the OX8 antibody). Proteins enriched over 2-fold with a p-value below 0.05 were considered significantly enriched.

Comparison between the anti- α2 and anti- α4s was done in the following way:

(1) Datasheet from the Proline export file, containing all the protein set entries with their relative abundance, called “Protein sets” was copied for treatment and the empty fields were replaced with zeros.

(2) Logical tests for every protein entry were performed, to determine if it was detected in at least 4 out of 8 analysis runs of at least one group of samples (4 samples times 2 technical replicates), then that it was determined by specific peptides, then filtered only the entries that satisfy the said tests. The logic tests were done on raw intensities, not the normalized ones.

(3) The technical replicates were averaged and the fifth percentile for every group was calculated.

(4) Number of missing values for each IP sample were calculated and the missing values were replaced by the fifth percentile for protein entries with two or more missing values.

(5) The iBAQ values were calculated by dividing the intensities with the number of observable peptides for each entry.

(6) Mean proteasome abundance was calculated as average of iBAQs for non-catalytic subunits of the proteasome, excluding the α4 and α4s.

(7) The iBAQ values were normalized in all the groups with mean proteasome value for each group.

(8) The one-sided paired T-test and fold change were calculated between the anti-α2 and anti-α4s groups. The comparison was done only for proteins significantly enriched between the experimental and control groups (see the end of previous paragraph).

<u>Estimation of the regulator stoichiometry of the α4- and α4s-containing proteasome :</u>

The composition of these two complexes can be estimated for known interactors based on their intensities in the two CoIPs that have a different ratio of enrichment of α4 and α4s, which is the case in our experiments (anti-α2 and anti-α4s CoIP). Firstly, we need to

know the ratio of α4 versus α4s in both CoIPs. The intensity of an interactor of a particular complex (α4- or α4s-containing proteasome) can be expressed via the following formulas:

$x=(A(\alpha 2)*d - A(\alpha 4s)*b)/(a*d - b*c)$

$y=(A(\alpha 2)*c - A(\alpha 4s)*a)/(b*c - a*d)$

if starting from statements:

$A(\alpha 2)=a*x+b*y$ AND $A(\alpha 4s)=c*x+d*y$

for a,b,c,d being the percentages in 0 to 1 format (e.g. 0.15 for 15%), where x is the intensity of a protein P bound to α4-containing P20S and y is the intensity of a protein P bound to α4s-containing P20S. A(α2) is the experimentally measured intensity of the protein P in the anti-α2 CoIP, while A(α4s) is the experimentally measured intensity of the protein P in the anti-α4s CoIP.

Additionally:

since $a=1-b$ AND $c=1-d$

then:

$x=(b*A(\alpha 4s) - d*A(\alpha 2))/(b-d)$

$y=((1-d)*A(\alpha 2) + (b-1)*A(\alpha 4s))/(b-d)$

(conditions: $b\neq d$, $bd\neq d$)

The estimations are easily derived when the two formulae are solved together, once the intensity values of a protein P for each CoIP are plugged in, together with the α4s percentage in each CoIP (b and d factors, 42% and 96% for anti-α2 and anti- α4s IP, respectively).

<u>Top-down LC-MSMS</u>

Nano-LC-MS analyses of commercial or immunopurified 20S were performed on a nanoRS UHPLC system (Dionex) coupled to an LTQ-Orbitrap Fusion Tribrid mass spectrometer (Thermo Fisher Scientific), as previously described (Lesne *et al.*, 2019). Briefly, a total of 5 µL of sample at 0.5 µM was loaded onto a reverse-phase C4-precolumn (300 µm i.d. × 5 mm; Thermo Fisher Scientific) at 20 µL/min in 2% acetonitrile (ACN) and 0.2% formic acid (FA). After 5 minutes of desalting, the precolumn was switched online with an analytical C4 nanocolumn (75 µm i.d. × 15 cm; in-house packed with C4 Reprosil) equilibrated in 95% solvent A (5% ACN, 0.2% FA) and 5% solvent B (0.2% FA in ACN). Proteins were eluted using a binary gradient ranging from 5% to 40% (5 minutes) and then 40% to 99% (33 minutes) of solvent B at a flow rate of 300 nL/min.

The Fusion Tribrid (Thermo Fisher Scientific) was operated in single MS acquisition mode with the Xcalibur software (Thermo Fisher Scientific). The spray voltage was set to 1900 V, the ion transfer tube temperature to 350°C, the RF lens to 60%, and no in-source dissociation was applied. The MS scans were acquired in the 700 to 2000 m/z range with the resolution set to 15 000 and using 10 µscans for averaging. LC-MS .raw files were automatically deconvoluted with the rolling window deconvolution software RoWinPro (Gersch *et al.*, 2015) and the proteoform footprints were visualized with VisioProt-MS v2.0 (Locard-Paulet *et al.*, 2019).

For MSMS acquisition, 3 second cycles were used, with the following MS parameters: MS scan range between 1000 and 2000 m/z in Orbitrap at 7,500 resolution, 10 µscans for averaging. MSMS activation (HCD) was done with 25% activation energy, with spectra acquisition in the Orbitrap at 60,000 resolution. The AGC target was set to 1e6. Dynamic exclusion for 600 s was used within 60 s to prevent repetitive selection of the same precursor (selection tolerance: ±10ppm) and improve the number of identified proteins. The following source settings were used: Spray voltage 1900V, RF lens 60%, no in-source fragmentation was used. The MSMS analysis of the degraded 20S proteasome used the same parameters, except for the activation method, whereby EThcD was used instead of HCD: ETD activation time of 5ms, ETD reagent target intensity set at 7e5, maximum ETD reagent injection time set at 200ms, with supplemental EThcD activation at 25% energy. The spectra identification was done in Proteome Discoverer (Thermo Fisher Scientific) v.2.3, using an Absolute Mass Search with the following parameters: precursor mass tolerance - 1000 Da, fragment mass tolerance - 15ppm. Mutations and truncations of the proteoforms were then manually curated. The search database was generated from the ensemble of the available Swiss-Prot and TrEMBL entries for bovin 20S proteasome, bovin proteasome regulators (19S, PA28 subunits, and PA200) and their isoforms.

<u>HDX-MS</u>

HDX-MS experiments were performed on a Synapt-G2Si (Waters Scientific, Manchester, UK) coupled to a Twin HTS PAL dispensing and labelling robot (Trajan Scientific, Milton Keynes, UK) via a NanoAcquity system with HDX technology (Waters, Manchester, UK). Data were collected with MassLynX v.4.1 (Waters Scientific (Manchester, UK) and the robot was controlled via HDX Director v.1.0.3.9 (LEAP Technologies, Carborro, NC, USA). Each step was optimized to minimize sample loss and work with such a heterogeneous sample, as described previously (Lesne *et al.*, 2020).

Briefly, 5.7 µL of bovin 20S proteasome at 2.3 µM were aspirated and 5.2 µL were diluted in 98.8 µL of protonated (peptide mapping) or deuterated buffer (20 mM Tris pH/pD 7.4, 1 mM EDTA, 1 mM DTT) and incubated at 20 °C for 0, 0.5, 1, 5, 10, and 30 min. The final

D2O percentage was 95% in the labelled samples. 99 µL were then transferred to vials containing 11 µL of precooled quenching solution (500 mM glycine at pH 2.3). After 30 s. of quenching, 105 µL were injected into a 100 µL loop. Proteins were digested online with a 2.1 × 30 mm Poros Immobilized Pepsin column (Life Technologies/Applied Biosystems, Carlsbad, CA, USA). The temperature of the digestion room was set at 15 °C.
Peptides were desalted for 3 min on a C18 pre-column (Acquity UPLC BEH 1.7 µm, VANGUARD) and separated on a C18 column (Acquity UPLC BEH 1.7 µm, 1.0 × 100 mm) by the following gradient: 5–35% buffer B (100% acetonitrile, 0.2% formic acid) for 12 min, 35–40% for 1 min, 40–95% for 1 min, 2 min at 95% followed by 2 cycles of 5–95% for 2 min and a final equilibration at 5% buffer A (5% acetonitrile, 0.2% formic acid) for 2 min. The total runtime was 25 min. The temperature of the chromatographic module was set at 4 °C. Experiments were run in triplicates and the protonated buffer was injected between each triplicate to wash the column and avoid cross-over contamination.
The acquisitions were performed in positive and resolution mode in the m/z range 50–2000 Th. The sample cone and capillary voltages were set at 30 and 3 kV, respectively. The analysis cycles for nondeuterated samples alternated between a 0.3 s low energy scan (Trap and Transfer collision energies set to 4 V and 2 V, respectively), a 0.3 sec high energy scan (Ramp Trap and Transfer collision energies set to 18 to 40 V and 2 to 2 V, respectively) and a 0.3 sec lockspray scan (0.1 µM [Glu1]-Fibrinopeptide in 50% acetonitrile, 50% water and 0.2% formic acid infused at 10 µL/min). The lockspray trap collision energy was set at 32 V and a GFP scan of 0.3 sec is acquired every min. Deuterated samples were acquired only with the low energy and lockspray functions.
Peptide identification was performed with ProteinLynx Global SERVER v.3.0.2 (PLGS, Waters, Manchester, UK) based on the MSE data acquired on the nondeuterated samples. The MSMS spectra were searched against a home-made database containing sequences of the 18 c20S, i20S and s20S subunits, all the 19S subunits, as well as the entries for PA28αβ, PA28γ and PA200 regulators, as well as pepsin from Sus scrofa. Peptides were filtered in DynamX v.3.0 from Waters Scientific (Manchester, UK) with the following parameters: peptides identified in at least two replicates, 0.2 fragments per amino-acid, intensity threshold 1000. The RDUs were not corrected for back exchange. These data were then used for structural data mining with HDX-Viewer (Bouyssié *et al.*, 2019). Molecular representations of Fig.6 and Fig.7 were generated in UCSF ChimeraX v.0.9 (Goddard et al., 2018) and Visual Molecular Dynamics (Humphrey, Dalke and Schulten, 1996), respectively.

Molecular Dynamics simulations and analysis

For molecular dynamics (MD simulations), we used the α4 model to perform an homology model of the bovine α4s subunit using the modeler program (Webb and Sali, 2016) (83.2 % sequence identity between α4 and α4s). For each structure, we then performed 1 µs of molecular dynamics (MD) simulations using GROMACS 2020 (Van Der Spoel *et al.*,

2005; Abraham *et al.*, 2015) in combination with AMBER14SB force field (Maier *et al.*, 2015). We first embedded each model in a waterbox using TIP3P water model (Jorgensen *et al.*, 1983). Cl ions were added to neutralize the system. Energy minimization was performed using the steepest descent algorithm and each system was equilibrated with a constant temperature (canonical ensemble, NVT, 300 K) ensemble for 100 picoseconds (ps), followed by a 100 ps equilibration at constant pressure (isothermal-isobaric, NPT, 1 bar). For equilibration steps, the protein backbone was kept constrained. For equilibration and production runs, we applied the velocity-rescaling thermostat (Bussi, Donadio and Parrinello, 2007) on protein and solvent, coupled with the Parrinello–Rahman barostat (Parrinello and Rahman, 1981), with a time constant of 2 ps and compressibility of 4.5x10-5 bar-1. Long-range electrostatics were modeled using the Particle-Mesh Ewald method (Darden, York and Pedersen, 1993; Essmann *et al.*, 1995). All bonds were treated using the LINCS algorithm (Hess, 2008). For both α4 and α4s models, we performed 1 µs of simulation at 300 K and ambient pressure of 1 bar with an integration time step of 2 femto-seconds.

We then analyzed the dynamics of the two last α-helices. We analyzed the creation of hydrogen bonds between water molecules and helices NH groups. To do so, we used VMD (Humphrey, Dalke and Schulten, 1996) Hbonds plugin (https://www.ks.uiuc.edu/Research/vmd/plugins/hbonds/) to count hydrogen bonds formed every 100 ps of the trajectory using a donor-acceptor distance of 3.5 Å and a cutoff angle of 30°. We then calculated the Solvent Accessible Surface Area (SASA) using VMD functions (https://www.ks.uiuc.edu/Research/vmd/vmd-1.8.3/ug/node121.html). To be comparable with HDX-MS data, only the NH groups of residues 180 to 189 and 225 to 241 were used for these two analyses. We calculated hydrogen bonds formed between the two helices (respectively residues 185 to 198 and 224 to 241) as well as the inter-helix angle θ every 100 ps. We used VMD Hbonds plugin and Tcl functions to calculate respectively interhelix hydrogen bonds and interhelix angle.

<u>Activity assays</u>

The assay was performed in 96-well black plates (Greiner Bio- One, UK). The 20S proteasome (1.25 µg of either c20S from muscle or testes 20S pool from testis) was mixed with 3 µg (or 0.75µg) of recombinant PA200 regulator (see below) in a total volume of 16 µL of Activity Buffer (20 mM Tris-HCl, 5 mM MgCl2, 2 mM ATP, 0.5 mM DTT) to obtain a molar ratio of 20S to PA200 to be either 1:8 or 1:2 and left to interact for 30 min at 37°C. The mix of complexes was then diluted to a total volume of 400 µL. The 20S alone (1.25 µg of either standard 20S from muscle or testes 20S pool from testis) was also diluted to a total volume of 400 µL. All the mixes were distributed in aliquots of 50 µL (or 25 µL of sample + 25 µL of Activity buffer for the assays of LLVY) to which 50 µL of Activity buffer was added, supplemented with 100 µM fluorogenic peptide substrate: Suc-LLVY-AMC,

Boc-LRR-AMC or z-LLE-AMC, to probe for chymotrypsin-, trypsin- or caspase-like activities, respectively. The kinetic assays were performed at 37 °C in a FLX-800 spectrofluorometer (BIOTEK) over 60 min with one reading every 5 min, at 360 nm for excitation and 460 nm for emission. The slope of the kinetic assay (fluorescence intensity = f (time)) and the quantity of proteasome were used to determine the proteasome specific chymotrypsin-like activity.

Pull-Down Assays

20S proteasomes were purified from bovine testes as already described above. It is established that the 20S pool contains ~50% s20S and ~50% α4-containing 20S. Purified recombinant human 19S complex was bought from R&D Systems (Minneapolis, USA), recombinant, FLAG-tagged human PI31 protein was bought from OriGene (Rockville, USA) and PA200 protein was prepared as described in (Toste Rêgo and da Fonseca, 2019).

The PI31 and 20S pool were mixed at a 10 to 1 ratio in Equilibration buffer 1 (20 mM Tris HCl, 1 mM EDTA, 10% glycerol, 100 mM NaCl, 2 mM ATP, 5 mM MgCl2, pH 7.6) in a total volume of 100µL, at final concentrations of 280nM 20S and 2.8µM PI31. The mix was incubated for 3,5h at 4°C with either the anti-FLAG resin or the proteinG MagBeads containing 100µg of anti-α2 antibody. The resin or the beads were washed with 5mL Equilibration buffer. The elution was done with 2x volume of the slurry of Glycine buffer (Glycine pH3,5 0,1 M) and the samples were prepared for LC-MS analysis on mini-S-trap cartridges (Protifi, Farmingdale NY USA) as recommended by the supplier. For FLAG-tag IP, 280 µL of 50% M2 anti-FLAG affinity resin slurry was used (Merck, Darmstadt, Germany). For anti-α2 IP, 100 µL of 25% MagBeads slurry were used (GenScript, Piscataway, NJ USA).

The PA200 of 19S were separately mixed with 20S pool in a 1:2 ratio (10 µg of 19S with 20 µg of 20S proteasome and 2.94 µg PA200 with 20 µg 20S proteasome) in the Equilibration buffer 2 (50 mM Tris pH 7.6, 1 mM MgCl2, 200 µM ATP, 0.5 M DTT) in a total volume of 24 µL. Both mixes were incubated for 30 min at 37 °C, then split in two halves. One half was mixed with the experimental group antibody (10 µg of anti-PSMC2 for 19S-20S mix or anti-PA200 for PA200-20S mix) or control group antibody (10 µg of anti-α2 antibody) and incubated for 30 min at 37°C. Each of the samples was then mixed with ProteinG MagBeads (50 µL 25% slurry per sample) and incubated overnight at 4 °C. The elution of complexes was done with 50 µL of S-Trap buffer and the samples were prepared for LC-MS analysis on mini-S-trap cartridges (Protifi, Farmingdale NY USA) as recommended by the supplier.

Experimental Design and Statistical Rationale

Label-free MS Analyses: All statistical analyses were performed on at least three independent biological replicates. For each biological replicate, results from at least two injection replicates were averaged. The analyses on bovine testes were done in four biological replicates. Probability values (p) were determined by one-way paired Student's test for groups of equal variance. Differences were statistically significant at confidence levels of 95% (*), 99% (**), or 99.9% (***). The Pull-Down assays were done in three technical replicates, with p values determined by two-sided, non-paired Student's test for groups of equal variance.
The "rat germ cells" dataset contains MS results from the analysis of the IPs and lysates of 4 cell types (Sertoli cells, spermatogonia, spermatocytes, spermatids) in biological triplicates (pools of cells from different individuals for each group), analysed in three injection replicates, for a total of 72 raw files. The "bovine testis CoIP" dataset contains MS results for 4 types of IPs (anti-PA200, anti-α2, anti-α4s, and OX-8 control) from four biological replicates, two technical injections per biological replicate, and lysates for each biological sample, for a total of 40 .raw files. The quantitative comparison of proteins was done based on normalized protein intensities from the "Protein groups" sheet in the Proline output file.

Acknowledgements

This work was supported by the French Ministry of Research (ANR-ProteasoRegMS to JM, Investissements d'Avenir Program, Proteomics French Infrastructure, ANR-10-INBS-08 to OB-S), University of Toulouse (grant to DZ), the Fonds Européens de Développement Régional Toulouse Métropole and the Région Midi-Pyrénées (OB-S). PCAdF and ATR were funded by the Medical Research Council (MC_UP_1201/5 grant to PCAdF).

ABBREVIATIONS

MWs - molecular weights

SEC - Size Exclusion Chromatography

UHPLC - Ultra High Performance Liquid Chromatography

IP - immunopurification

TDP - Top-Down Proteomics

BUP - Bottom-Up Proteomics

s20S - spermatoproteasome

c20S - standard proteasome

i20S - immunoproteasome

iBAQ – intensity-based absolute quantification (a value obtained by dividing the sum of peptide abundances by the number of theoretically observable peptides of a protein. It is a normalized protein intensity that permits comparing protein copy numbers - biologically more descriptive value than Label-Free Quantification (LFQ) intensity which is only related to signal intensity)

References

Ahuja, J. S. *et al.* (2017) 'Control of meiotic pairing and recombination by chromosomally tethered 26 S proteasome', *Science*, 355(6323), pp. 408–411. doi: 10.1126/science.aaf4778.

Aristizábal, D. *et al.* (2019) 'Heat stress reveals high molecular mass proteasomes in Arabidopsis thaliana suspension cells cultures', *Plant Physiology and Biochemistry*, 140, pp. 78–87. doi: 10.1016/j.plaphy.2019.04.034.

Bader, M. *et al.* (2011) 'A conserved F box regulatory complex controls proteasome activity in Drosophila', *Cell*. Elsevier Inc., 145(3), pp. 371–382. doi: 10.1016/j.cell.2011.03.021.

Banerjee, S., Kumar, M. and Wiener, R. (2020) 'Decrypting UFMylation: How proteins are modified with UFM1', *Biomolecules*, 10(10), pp. 1–14. doi: 10.3390/biom10101442.

Bassermann, F., Eichner, R. and Pagano, M. (2014) 'The ubiquitin proteasome system — Implications for cell cycle control and the targeted treatment of cancer', *Biochimica et Biophysica Acta (BBA) - Molecular Cell Research*, 1843(1), pp. 150–162. doi: 10.1016/j.bbamcr.2013.02.028.

Baumeister, W. *et al.* (1998) 'The Proteasome: Paradigm of a Self-Compartmentalizing Protease', *Cell*, 92(3), pp. 367–380. doi: 10.1016/S0092-8674(00)80929-0.

Blickwedehl, J. *et al.* (2008) 'Role for proteasome activator PA200 and postglutamyl proteasome activity in genomic stability', *Proceedings of the National Academy of Sciences of the United States of America*, 105(42), pp. 16165–16170. doi: 10.1073/pnas.0803145105.

Bolcun-Filas, E. and Handel, M. A. (2018) 'Meiosis: the chromosomal foundation of reproduction', *Biology of Reproduction*, 99(1), pp. 112–126. doi: 10.1093/biolre/ioy021.

Bose, R. *et al.* (2014) 'Ubiquitin–Proteasome System in Spermatogenesis', in *Advances in Experimental Medicine and Biology*, pp. 181–213. doi: 10.1007/978-1-4939-0817-2_9.

Bousquet-Dubouch, M.-P. *et al.* (2009) 'Affinity Purification Strategy to Capture Human Endogenous Proteasome Complexes Diversity and to Identify Proteasome-interacting Proteins', *Molecular & Cellular Proteomics*, 8(5), pp. 1150–1164. doi: 10.1074/mcp.M800193-MCP200.

Bouyssié, D. *et al.* (2020) 'Proline: an efficient and user-friendly software suite for large-scale proteomics', *Bioinformatics*. Edited by A. Valencia, 36(10), pp. 3148–3155. doi: 10.1093/bioinformatics/btaa118.

Calvel, P. *et al.* (2010) 'Testicular postgenomics: targeting the regulation of spermatogenesis',

Philosophical Transactions of the Royal Society B: Biological Sciences, 365(1546), pp. 1481–1500. doi: 10.1098/rstb.2009.0294.

Cho-Park, P. F. and Steller, H. (2013) 'Proteasome regulation by ADP-ribosylation', *Cell*. Elsevier Inc., 153(3), pp. 614–627. doi: 10.1016/j.cell.2013.03.040.

Com, E. *et al.* (2003) 'New Insights into the Rat Spermatogonial Proteome', *Molecular & Cellular Proteomics*, 2(4), pp. 248–261. doi: 10.1074/mcp.M300010-MCP200.

De, M. *et al.* (2003) 'β2 Subunit Propeptides Influence Cooperative Proteasome Assembly', *Journal of Biological Chemistry*, 278(8), pp. 6153–6159. doi: 10.1074/jbc.M209292200.

Døskeland, A. P. (2006) 'A method for simple identification of signature peptides derived from polyUb-K48 and K63 by MALDI-TOF MS and chemically assisted MS/MS fragmentation.', *Amino acids*, 30(1), pp. 99–103. doi: 10.1007/s00726-005-0227-4.

Fabre, B. *et al.* (2013) 'Subcellular Distribution and Dynamics of Active Proteasome Complexes Unraveled by a Workflow Combining in Vivo Complex Cross-Linking and Quantitative Proteomics', *Molecular & Cellular Proteomics*, 12(3), pp. 687–699. doi: 10.1074/mcp.M112.023317.

Fabre, B. *et al.* (2014) 'Label-Free Quantitative Proteomics Reveals the Dynamics of Proteasome Complexes Composition and Stoichiometry in a Wide Range of Human Cell Lines', *Journal of Proteome Research*, 13(6), pp. 3027–3037. doi: 10.1021/pr500193k.

Fabre, B. *et al.* (2015) 'Deciphering preferential interactions within supramolecular protein complexes: the proteasome case', *Molecular Systems Biology*, 11(1), p. 771. doi: 10.15252/msb.20145497.

Finley, D. (2009) 'Recognition and Processing of Ubiquitin-Protein Conjugates by the Proteasome', *Annual Review of Biochemistry*, 78(1), pp. 477–513. doi: 10.1146/annurev.biochem.78.081507.101607.

Gao, X. *et al.* (2019) 'The REGγ-Proteasome Regulates Spermatogenesis Partially by P53-PLZF Signaling', *Stem Cell Reports*. Elsevier, 13(3), pp. 559–571. doi: 10.1016/j.stemcr.2019.07.010.

Gersch, M. *et al.* (2015) 'A Mass Spectrometry Platform for a Streamlined Investigation of Proteasome Integrity, Posttranslational Modifications, and Inhibitor Binding', *Chemistry & Biology*, 22(3), pp. 404–411. doi: 10.1016/j.chembiol.2015.01.004.

Goddard, T. D. *et al.* (2018) 'UCSF ChimeraX: Meeting modern challenges in visualization and analysis', *Protein Science*, 27(1), pp. 14–25. doi: 10.1002/pro.3235.

Gomez-H, L. *et al.* (2019) *The PSMA8 subunit of the spermatoproteasome is essential for proper meiotic exit and mouse fertility*, *PLoS Genetics*. doi: 10.1371/journal.pgen.1008316.

Griffin, T. A. *et al.* (1998) 'Immunoproteasome Assembly: Cooperative Incorporation of Interferon γ (IFN-γ)–inducible Subunits', *Journal of Experimental Medicine*, 187(1), pp. 97–104. doi: 10.1084/jem.187.1.97.

Groettrup, M. *et al.* (1997) 'The subunits MECL-1 and LMP2 are mutually required for

incorporation into the 20S proteasome', *Proceedings of the National Academy of Sciences*, 94(17), pp. 8970–8975. doi: 10.1073/pnas.94.17.8970.

Guillaume, B. *et al.* (2010) 'Two abundant proteasome subtypes that uniquely process some antigens presented by HLA class I molecules', *Proceedings of the National Academy of Sciences*, 107(43), pp. 18599–18604. doi: 10.1073/pnas.1009778107.

Heink, S. *et al.* (2005) 'From The Cover: IFN- -induced immune adaptation of the proteasome system is an accelerated and transient response', *Proceedings of the National Academy of Sciences*, 102(26), pp. 9241–9246. doi: 10.1073/pnas.0501711102.

Holstein, A. F., Schulze, W. and Davidoff, M. (2003) 'Understanding spermatogenesis is a prerequisite for treatment', *Reproductive Biology and Endocrinology*, 1, pp. 1–16. doi: 10.1186/1477-7827-1-107.

Hou, C. C. and Yang, W. X. (2013) 'New insights to the ubiquitin-proteasome pathway (UPP) mechanism during spermatogenesis', *Molecular Biology Reports*, 40(4), pp. 3213–3230. doi: 10.1007/s11033-012-2397-y.

Hsu, P. J. *et al.* (2017) 'Ythdc2 is an N6-methyladenosine binding protein that regulates mammalian spermatogenesis', *Cell Research*, 27(9), pp. 1115–1127. doi: 10.1038/cr.2017.99.

Huang, L. *et al.* (2016) 'Proteasome activators, PA28γ and PA200, play indispensable roles in male fertility', *Scientific Reports*, 6(1), p. 23171. doi: 10.1038/srep23171.

Humphrey, W., Dalke, A. and Schulten, K. (1996) 'VMD: Visual molecular dynamics', *Journal of Molecular Graphics*, 14(1), pp. 33–38. doi: 10.1016/0263-7855(96)00018-5.

Hunter, N. (2015) 'Meiotic Recombination: The Essence of Heredity', *Cold Spring Harbor Perspectives in Biology*, 7(12), p. a016618. doi: 10.1101/cshperspect.a016618.

Hutchins, E. D. *et al.* (2016) 'Differential expression of conserved and novel microRNAs during tail regeneration in the lizard Anolis carolinensis', *BMC Genomics*, 17(1), p. 339. doi: 10.1186/s12864-016-2640-3.

Johnston-Carey, H. K., Pomatto, L. C. D. and Davies, K. J. A. (2016) 'The Immunoproteasome in oxidative stress, aging, and disease', *Critical Reviews in Biochemistry and Molecular Biology*, 51(4), pp. 268–281. doi: 10.3109/10409238.2016.1172554.

Kelstrup, C. D. *et al.* (2018) 'Performance Evaluation of the Q Exactive HF-X for Shotgun Proteomics', *Journal of Proteome Research*, 17(1), pp. 727–738. doi: 10.1021/acs.jproteome.7b00602.

Khor, B. *et al.* (2006) 'Proteasome Activator PA200 Is Required for Normal Spermatogenesis', *Molecular and Cellular Biology*, 26(8), pp. 2999–3007. doi: 10.1128/MCB.26.8.2999-3007.2006.

Kim, M.-S. *et al.* (2014) 'A draft map of the human proteome', *Nature*, 509(7502), pp. 575–581. doi: 10.1038/nature13302.

Kingsbury, D. J., Griffin, T. A. and Colbert, R. A. (2000) 'Novel Propeptide Function in 20 S Proteasome Assembly Influences β Subunit Composition', *Journal of Biological Chemistry*,

275(31), pp. 24156–24162. doi: 10.1074/jbc.M001742200.

Kirk, R. *et al.* (2008) 'Structure of a conserved dimerization domain within the F-box protein Fbxo7 and the PI31 proteasome inhibitor', *Journal of Biological Chemistry*, 283(32), pp. 22325–22335. doi: 10.1074/jbc.M709900200.

Kloetzel, P.-M. (2004) 'The proteasome and MHC class I antigen processing', *Biochimica et Biophysica Acta (BBA) - Molecular Cell Research*, 1695(1–3), pp. 225–233. doi: 10.1016/j.bbamcr.2004.10.004.

Kniepert, A. and Groettrup, M. (2014) 'The unique functions of tissue-specific proteasomes', *Trends in Biochemical Sciences*. Elsevier Ltd, 39(1), pp. 17–24. doi: 10.1016/j.tibs.2013.10.004.

Lake, C. M. and Hawley, R. S. (2016) 'Seminars in Cell & Developmental Biology Becoming a crossover-competent DSB', *Seminars in Cell and Developmental Biology*. Elsevier Ltd, 54, pp. 117–125. Available at: http://dx.doi.org/10.1016/j.semcdb.2016.01.008.

Lesne, J. *et al.* (2019) 'Top-Down and Intact Protein Mass Spectrometry Data Visualization for Proteoform Analysis Using VisioProt-MS', *Bioinformatics and Biology Insights*. SAGE Publications Inc., 13, p. 117793221986822. doi: 10.1177/1177932219868223.

Lesne, J. *et al.* (2020) 'Conformational maps of human 20S proteasomes reveal PA28- and immuno-dependent inter-ring crosstalks', *Nature Communications*, 11(1), p. 6140. doi: 10.1038/s41467-020-19934-z.

Li, X. *et al.* (2014) 'Molecular and Cellular Roles of PI31 (PSMF1) Protein in Regulation of Proteasome Function', *Journal of Biological Chemistry*, 289(25), pp. 17392–17405. doi: 10.1074/jbc.M114.561183.

Liu, K. *et al.* (2019) 'PI31 Is an Adaptor Protein for Proteasome Transport in Axons and Required for Synaptic Development', *Developmental Cell*, 50(4), pp. 509-524.e10. doi: 10.1016/j.devcel.2019.06.009.

Locard-Paulet, M. *et al.* (2019) 'VisioProt-MS: interactive 2D maps from intact protein mass spectrometry', *Bioinformatics*. Edited by A. Valencia, 35(4), pp. 679–681. doi: 10.1093/bioinformatics/bty680.

Menneteau, T. *et al.* (2019) 'Mass Spectrometry-based Absolute Quantification of 20S Proteasome Status for Controlled Ex-vivo Expansion of Human Adipose-derived Mesenchymal Stromal/Stem Cells', *Molecular & Cellular Proteomics*, 18(4), pp. 744–759. doi: 10.1074/mcp.RA118.000958.

Meziane, E. K. *et al.* (2011) 'Knockdown of Fbxo7 reveals its regulatory role in proliferation and differentiation of haematopoietic precursor cells', *Journal of Cell Science*, 124(13), pp. 2175–2186. doi: 10.1242/jcs.080465.

Min, M. and Lindon, C. (2012) 'Substrate targeting by the ubiquitin–proteasome system in mitosis', *Seminars in Cell & Developmental Biology*, 23(5), pp. 482–491. doi: 10.1016/j.semcdb.2012.01.015.

Minis, A. *et al.* (2019) 'The proteasome regulator PI31 is required for protein homeostasis,

synapse maintenance, and neuronal survival in mice', *Proceedings of the National Academy of Sciences*. National Academy of Sciences, 116(49), pp. 24639–24650. doi: 10.1073/PNAS.1911921116.

Nelson, D. E., Randle, S. J. and Laman, H. (2013) 'Beyond ubiquitination: the atypical functions of Fbxo7 and other F-box proteins.', *Open biology*, 3(10), p. 130131. doi: 10.1098/rsob.130131.

Paraskevopoulos, K. *et al.* (2014) 'Dss1 Is a 26S Proteasome Ubiquitin Receptor', *Molecular Cell*, 56(3), pp. 453–461. doi: 10.1016/j.molcel.2014.09.008.

Pineau, C. *et al.* (no date) 'Germ cell-conditioned medium contains multiple factors that modulate the secretion of testins, clusterin, and transferrin by Sertoli cells.', *Journal of andrology*, 14(2), pp. 87–98. Available at: http://www.ncbi.nlm.nih.gov/pubmed/8514623.

Prasada Rao, H. B. D. *et al.* (2017) 'A SUMO-ubiquitin relay recruits proteasomes to chromosome axes to regulate meiotic recombination', *Science*, 355(6323), pp. 403–407. doi: 10.1126/science.aaf6407.

Qian, M.-X. *et al.* (2013) 'Acetylation-Mediated Proteasomal Degradation of Core Histones during DNA Repair and Spermatogenesis', *Cell*, 153(5), pp. 1012–1024. doi: 10.1016/j.cell.2013.04.032.

Rathje, C. C. *et al.* (2019) 'A Conserved Requirement for Fbxo7 During Male Germ Cell Cytoplasmic Remodeling', *Frontiers in Physiology*, 10(October), pp. 1–16. doi: 10.3389/fphys.2019.01278.

Sbardella, D. *et al.* (2018) 'The insulin-degrading enzyme is an allosteric modulator of the 20S proteasome and a potential competitor of the 19S', *Cellular and Molecular Life Sciences*, 75(18), pp. 3441–3456. doi: 10.1007/s00018-018-2807-y.

Sharon, M. *et al.* (2007) 'Mass Spectrometry Reveals the Missing Links in the Assembly Pathway of the Bacterial 20 S Proteasome', *Journal of Biological Chemistry*, 282(25), pp. 18448–18457. doi: 10.1074/jbc.M701534200.

Skinner, M. K. and Fritz, I. B. (1985) 'Structural characterization of proteoglycans produced by testicular peritubular cells and Sertoli cells.', *The Journal of biological chemistry*, 260(21), pp. 11874–83. Available at: http://www.ncbi.nlm.nih.gov/pubmed/3930486.

Skinner, O. S. *et al.* (2016) 'An informatic framework for decoding protein complexes by top-down mass spectrometry', *Nature Methods*, 13(3), pp. 237–240. doi: 10.1038/nmeth.3731.

Smith, L. M. and Kelleher, N. L. (2013) 'Proteoform: A single term describing protein complexity', *Nature Methods*. Nature Publishing Group, 10(3), pp. 186–187. doi: 10.1038/nmeth.2369.

Sohn, D. *et al.* (2006) 'The Proteasome Is Required for Rapid Initiation of Death Receptor-Induced Apoptosis', *Molecular and Cellular Biology*, 26(5), pp. 1967–1978. doi: 10.1128/MCB.26.5.1967-1978.2006.

Stadtmueller, B. M. and Hill, C. P. (2011) 'Proteasome Activators', *Molecular Cell*, 41(1), pp. 8–19. doi: 10.1016/j.molcel.2010.12.020.

Thompson, J. D., Schaeffer-Reiss, C. and Ueffing, M. (2008) *Functional Proteomics*, *Methods in*

molecular biology (Clifton, N.J.). Edited by J. D. Thompson, M. Ueffing, and C. Schaeffer-Reiss. Totowa, NJ: Humana Press (Methods in Molecular Biology). doi: 10.1007/978-1-59745-398-1.

Toebosch, A. M. *et al.* (1989) 'Effects of FSH and testosterone on highly purified rat Sertoli cells: inhibin alpha-subunit mRNA expression and inhibin secretion are enhanced by FSH but not by testosterone.', *The Journal of endocrinology*, 122(3), pp. 757–62. Available at: http://www.ncbi.nlm.nih.gov/pubmed/2509618.

Toste Rêgo, A. and da Fonseca, P. C. A. (2019) 'Characterization of Fully Recombinant Human 20S and 20S-PA200 Proteasome Complexes', *Molecular Cell*, 76(1), pp. 138-147.e5. doi: 10.1016/j.molcel.2019.07.014.

Uechi, H., Hamazaki, J. and Murata, S. (2014) 'Characterization of the testis-specific proteasome subunit α4s in mammals', *Journal of Biological Chemistry*, 289(18), pp. 12365–12374. doi: 10.1074/jbc.M114.558866.

Vimer, S. *et al.* (2020) 'Comparative Structural Analysis of 20S Proteasome Ortholog Protein Complexes by Native Mass Spectrometry', *ACS Central Science*, 6(4), pp. 573–588. doi: 10.1021/acscentsci.0c00080.

Wang, X. and Huang, L. (2007) 'Identifying Dynamic Interactors of Protein Complexes by Quantitative Mass Spectrometry', *Molecular & Cellular Proteomics*, 7(1), pp. 46–57. doi: 10.1074/mcp.M700261-MCP200.

Widjaja, C. E. *et al.* (2017) 'Proteasome activity regulates CD8+ T lymphocyte metabolism and fate specification', *Journal of Clinical Investigation*, 127(10), pp. 3609–3623. doi: 10.1172/JCI90895.

Wojtas, M. N. *et al.* (2017) 'Regulation of m6A Transcripts by the 3'→5' RNA Helicase YTHDC2 Is Essential for a Successful Meiotic Program in the Mammalian Germline', *Molecular Cell*. Elsevier Inc., 68(2), pp. 374-387.e12. doi: 10.1016/j.molcel.2017.09.021.

Wolf-Levy, H. *et al.* (2018) 'Revealing the cellular degradome by mass spectrometry analysis of proteasome-cleaved peptides', *Nature Biotechnology*. Nature Publishing Group, 36(11), pp. 1110–1116. doi: 10.1038/nbt.4279.

Wu, J., Peled-Zehavi, H. and Galili, G. (2020) 'The m6A reader ECT2 post-transcriptionally regulates proteasome activity in Arabidopsis', *New Phytologist*, 228(1), pp. 151–162. doi: 10.1111/nph.16660.

Yu, C. *et al.* (2019) 'Probing H2O2-mediated Structural Dynamics of the Human 26S Proteasome Using Quantitative Cross-linking Mass Spectrometry (QXL-MS)', *Molecular & Cellular Proteomics*, 18(5), pp. 954–967. doi: 10.1074/mcp.TIR119.001323.

Zhang, Q. *et al.* (2019) 'Meiosis I progression in spermatogenesis requires a type of testis-specific 20S core proteasome', *Nature Communications*. Springer US, 10(1), p. 3387. doi: 10.1038/s41467-019-11346-y.

Zhang, Z.-H. *et al.* (2021) 'Proteasome subunit α4s is essential for formation of spermatoproteasomes and histone degradation during meiotic DNA repair in spermatocytes', *Journal of Biological Chemistry*, 296(1), p. 100130. doi: 10.1074/jbc.ra120.016485.